

NH-rich organic compounds from the carbonaceous asteroid (162173) Ryugu: nanoscale spectral and isotopic characterizations

*L. G. Vacher¹, V. T. H. Phan¹, L. Bonal¹, M. Iskakova², O. Poch¹, P. Beck¹, E. Quirico¹, & R. C. Ogliore²

*Corresponding author: lionel.vacher@univ-grenoble-alpes.fr

¹Univ. Grenoble Alpes, CNRS, IPAG, 38000 Grenoble, France

²Department of Physics, Washington University in St. Louis, St. Louis, MO, USA.

Abstract

C-type asteroids, such as asteroid (162173) Ryugu, may have played a key role in delivering light elements and prebiotic organic materials to early Earth. The detection of spectral bands at 3.06 μm by MicrOmega, combined with the chemical identification of other NH-containing organic molecules in Ryugu samples, suggests the presence of potential NH-bearing compounds. However, the chemical forms of these NH-rich compounds—whether associated with N-rich organics, ammonium (NH_4^+) salts, NH_4 or NH-organics-bearing phyllosilicates, or other forms—remain to be better understood. In this study, we report the characterization of two Ryugu particles (C0050 and C0052) using multi-scale infrared (spectro-gonio-radiometric mm-reflectance, μ -FTIR, and nano-AFM-IR) and NanoSIMS techniques to constrain the nature and origin of NH-bearing components in the Ryugu asteroid. Our findings show that Ryugu's C0052 particle contains rare (~1 vol.%), micrometer-sized NH-rich organic compounds with peaks at 1660 cm^{-1} (mainly due to C=O stretching of the amide I band) and 1550 cm^{-1} (mainly due to N-H bending vibration mode of the amide II band), indicative of amide-related compounds. In contrast, these compounds are absent in C0050. Notably, nitrogen (N) isotopic analysis reveals that these amides in C0052 are depleted in ^{15}N ($\delta^{15}\text{N} = -215 \pm 92 \text{ ‰}$, 2σ), confirming their indigenous origin, while carbon (C) and hydrogen (H) isotopic compositions are indistinguishable from terrestrial values within errors ($\delta^{13}\text{C} = -22 \pm 52 \text{ ‰}$ and $\delta\text{D} = 194 \pm 368 \text{ ‰}$). The amides detected in C0052 could have formed through hydrothermal alteration from carboxylic acids and amines precursors on the Ryugu's parent planetesimal. Alternatively, they could have originated from the irradiation of ^{15}N -depleted N-bearing ice by UV light or galactic cosmic rays (GCR), either at the surface of the asteroid in the outer Solar System or on mantle of interstellar dust grains in the interstellar medium (ISM). Amides delivered to early Earth by primitive small bodies, such as asteroid Ryugu, may have played a crucial role in prebiotic chemistry.

Submitted to *Meteoritics and Planetary Science* – December 26, 2024

1. Introduction

In December 2019, the JAXA Hayabusa2 spacecraft returned to Earth samples from both the surface (Chamber A) and sub-surface (Chamber C) of the near-Earth carbonaceous (C-type) asteroid (162173) Ryugu (Watanabe et al., 2019; Tachibana et al., 2022). Preliminary laboratory analyses revealed that these samples are mineralogically, chemically, and isotopically similar to rare volatile-rich Ivuna-type carbonaceous (CI) chondrites (Hopp et al., 2022; Yada et al., 2022), whose average compositions are similar to that of the solar photosphere (Palme et al., 2014). The returned samples provide strong evidence of significant aqueous alteration, as seen by the widespread occurrence of secondary minerals, including phyllosilicates (serpentinite and saponite), dolomite, magnetite, and pyrrhotite. These minerals likely formed through low-temperature (<100°C) fluid circulation on the parent asteroid (T. Nakamura et al., 2022; Yada et al., 2022; Ito et al., 2022). Organic matter (OM), accounting for ~3 wt.% of the total mass of the studied particles (Yabuta et al., 2023), shares characteristics with OM found in other carbonaceous chondrites (Dartois et al., 2023; Naraoka et al., 2023; Bonal et al., 2024; Quirico et al., 2024). The OM is dispersed throughout the matrix, primarily as diffuse intergranular matter associated with phyllosilicates and nanoglobules (Yabuta et al., 2023; Phan et al., 2024; Stroud et al., 2024), suggesting that OM synthesis and preservation occurred under low-temperature aqueous conditions within the Ryugu's parent planetesimal (Potiszil et al., 2023).

MicrOmega reflectance spectra and Fourier Transform InfraRed spectroscopy (FTIR) measurements of Ryugu particles acquired at the Curation Center (Japan), reveal absorption bands at 3.06 μm and 3.24 μm on a few particles and a faint but global ~3.06-μm band on the entire grain collection. These absorption bands are attributed to N-H bond vibrational modes in NH-rich compounds (Pilorget et al., 2022; Yada et al., 2022). These compounds could be NH₄ phyllosilicates, NH₄ hydrated salts, and/or NH-rich organic molecules (e.g., amines or amides) possibly trapped within the interlayer spaces of phyllosilicates in Ryugu samples (Viennet et al. 2023). Since this first compositional analysis via infrared (IR) spectroscopy, NH-bearing organic molecules have been firmly detected in Ryugu samples via analytical chemistry (Yoshimura et al., 2023; Takano et al., 2024). However, whether these organic molecules, along with other NH-rich compounds, contribute to the global ~3.06-μm band detected in Ryugu remains to be investigated. Identifying the nature and distribution of NH-rich phases in Ryugu samples is crucial for constraining the N reservoirs that made up primitive small bodies (Füri and Marty, 2015; Hily-Blant et al., 2019; Grewal, 2022). For instance, NH₄⁺ has been detected at the surfaces of the dwarf planet Ceres, mainly associated to phyllosilicates (King et al., 1992; De Sanctis et al., 2015), and also on the surface and dust grains of comet 67P/Churyumov-Gerasimenko, in the form of NH₄⁺ salts (Poch et al., 2020; Altwegg et al., 2020, 2022).

While conventional IR methods can analyze the functional groups of C and N in Ryugu particles down to a size of $\sim 25 \times 25 \mu\text{m}^2$ using a GLOBAR thermal light source, novel IR techniques with nanoscale spatial resolution, such as atomic force microscope-based infrared spectroscopy (AFM-IR), can overcome the diffraction limit and identify mineral or organic phases at the nanometer scale (Mathurin et al., 2019; Kebukawa et al., 2019b; Phan et al., 2022, 2024). Coordinated analyses of AFM-IR and nanoscale secondary ion mass spectrometry (NanoSIMS) offer a new powerful approach (Kebukawa et al., 2023), enabling the identification and isotopic characterization of NH-rich compounds in Ryugu grains at similar spatial resolutions to constrain their origins and evolutionary history.

In this study, we report bulk and *in-situ* characterization of several fragments extracted from two Ryugu particles (C0050 and C0052) using multi-scale (millimeter to nanometer) IR techniques, including reflectance spectroscopy (using the SHADOW spectro-gonio-radiometer), transmission spectroscopy (μ -FTIR), and AFM-IR, to search for NH-bearing components in Ryugu particles. We also combined AFM-IR and NanoSIMS microscale techniques to investigate the C, N, and H isotopic composition of NH-rich organic compounds. Our findings provide insights into the nature and isotopic composition of these NH-rich compounds in Ryugu samples and offer a better understanding of the potential origin and formation processes of these compounds.

2. Methods

2.1. Selection of Hayabusa2 particles and sample preparation

The selection process of the Ruygu particles available for Announcement of Opportunity (AO) allocation was made using the FTIR spectra available in the Ryugu Sample Database in January 2022, as detailed in supplementary material S1. Briefly, to avoid spectral ambiguities related to the fact that carbonate and NH₄⁺ can have spectral absorptions at similar location around 3.4 μm and 7 μm (Lin-Vien et al., 1991; Petit et al., 2006), we have selected five particles whose FTIR spectra show no carbonate absorption band from about 3.8 μm to 4.0 μm (Figure S1). The Japan Aerospace Exploration Agency (JAXA) curation team allocated to our consortium the particles C0050 (2.2 mg) and C0052 (2.1 mg), which were then sent to the Institut de Planétologie et d’Astrophysique de Grenoble (IPAG, France), arriving in September 2022.

To prevent contamination, the Hayabusa2 sealed containers were opened in a controlled environment, using a glove bag flushed with N₂ (RH ≤ 5 % and O₂ < 0.1 %). The bulk particles were then transferred to a vacuum sapphire viewport for reflectance analysis. After the initial reflectance analysis, the particles were gently crushed in the glove bag. Small fragments were selected, crushed between diamond windows, and then placed in an environmental cell for transmission μ-FTIR analysis. Following transmission analysis, the environmental cell was opened, and the diamond windows were transferred into the AFM-IR at IPAG to detect IR vibrational signatures at the nanometer scale. After AFM-IR investigations, the diamond windows were coated with gold and subjected to Scanning Electron Microscope (SEM) investigations (Figure S2). After SEM observations, the coated diamond windows were then mounted on an in-house NanoSIMS holders for isotopic characterizations at the Laboratory for Space Sciences at Washington University (Wash U) in St. Louis (MO, USA).

2.2. Reflectance Spectroscopy (SHADOWS)

Reflectance spectra of particles C0050 and C0052 were acquired between 2 μm to 4.2 μm using the spectro-gonio radiometer SHADOWS (Spectrophotometer with cHanging Angles for the Detection of Weak Signals, Potin et al. 2018). This instrument is specially designed to measure dark samples with weak reflectance spectra from the visible to the near-infrared (350–5000 nm). The samples were illuminated with a beam ≤1.7 mm in diameter, at normal incidence (0°), and with an emergence angle of 30° (Potin et al., 2018). The spectrum was sampled every 20 nm, and the spectral resolution was 20 nm from 1.60 μm to 2.82 μm, and 41 nm from 2.84 μm to 4.20 μm. Surfaces of Spectralon and Infragold (LabSphere Inc.) were measured, from 0.38 μm to 2.00 μm and from 1.20 μm to 4.8 μm, respectively, under the same conditions

as the samples and used as references to calibrate the signal measured on the samples and obtain absolute values of reflectance factors, as described in Potin et al. (2018).

2.3. Micro-FTIR Spectroscopy (μ -FTIR)

The IR spectra were collected using a Bruker Hyperion 3000 IR microscope equipped with a liquid N₂ cooled mercury–cadmium–telluride (MCT) detector at IPAG. A 15 \times objective lens was used to focus the IR beam onto the samples, with a maximum spot size of 100 \times 100 μm^2 . Spectral resolution was set at 4 cm^{-1} across the range of 4000–650 cm^{-1} . Fragments from both particles of typically ~50–100 μm in size were manually selected inside a N₂-flushed glove bag using an Olympus SZX16 stereomicroscope, then were transferred onto a 3 \times 0.5 mm diamond window and crushed with another window using a custom press designed at IPAG. These windows were either placed in a custom environmental chamber to maintain a controlled atmosphere or analyzed directly in air. Spectral data were processed using in-house MATLAB code or Igor Wavemetrics, with baseline corrections applied via the “Baseline Fit” Matlab function. Normalization was performed by setting the absorbance of the Si-O peak (~1000 cm^{-1}) to 1.

2.4. Atomic Force Microscope-Based Infrared Spectroscopy (AFM-IR)

AFM-IR analyses were conducted on Ryugu samples following μ -FTIR measurements in a dry compressed air environment. Using a nanoIR3s system (Bruker) at IPAG, this technique enabled nanoscale IR imaging and absorption spectra collection. The system’s AFM probe generated topographical images and measured IR absorption via photo-thermal expansion. The excitation laser source, a Carmina laser (APE GmbH, Germany) covered the mid-IR range (2000–700 cm^{-1}), while the Firefly (FF) IR laser (M Squared, UK) provide light in the 2700–4000 cm^{-1} .

Two modes – Contact Mode (CM) and Tapping IR Mode (TM) were used for spectroscopy and imaging. Laser intensity and alignment were optimized before data collection. For AFM-IR imaging, the APE laser was used in TM mode with a laser power ranging of 25–40 % and a pulse rate of 340–400 kHz, conditions optimized to prevent damage to macromolecular organics due to laser irradiation. The analytical protocol employed in this study was validated in previous works on meteorites and coals (Phan et al., 2022, 2023, 2024).

AFM-IR images were collected across specific wavenumber ranges, including 2000–700 cm^{-1} for carbonyl (C=O) stretching, sp² aromatic (C=C), N-H bending mode, methylene (CH₂), and/or carbonate and/or NH₄⁺ bending mode, and silicate (Si-O) stretching. Images at 1660 cm^{-1} and 1550 cm^{-1} were also obtained to explore double peaks in these absorption bands, potentially indicating organic compounds like amide groups (e.g., -C(=O)-NH-). In the 3800–2700 cm^{-1} range, AFM-IR images were captured in CM using the Firefly laser targeting absorption bands related to –OH stretching (3600–3700 cm^{-1}), asymmetric

stretching of CH₃ (2960 cm⁻¹), asymmetric stretching of CH₂ (2930 cm⁻¹), symmetric stretching of CH₃ (2880 cm⁻¹), and symmetric stretching of CH₂ (2860 cm⁻¹). To visualize the spatial distribution of these components, composite RGB color images were generated by superimposing absorption images using Analysis Studio and MountainMapSPIP@ software. Images were realigned to correct for thermal drifts with the scan speeds set to 0.1 Hz, and scan sizes ranging from 300 × 300 points to 500 × 500 points depending on the Region of Interest (ROI).

Single-point AFM-IR spectra were obtained for Ryugu grains, C0052 and C0050 using CM with both the APE laser (2000–700 cm⁻¹) and the FF laser (3800–2700 cm⁻¹) for comprehensive analysis. To ensure high-quality spectra and preserve sample integrity, low laser power (1.22–5.03%) and a pulse rate of 240–300 kHz were maintained (Phan et al., 2022, 2023, 2024). Spectra were optimized with constant laser power, detected via an IR-sensitive photodetector with a wavenumber spacing of 4 cm⁻¹, co-averages of three spectra and five spectra for APE and FF lasers. For the 2000–700 cm⁻¹ range, a gold-coated semi-tap probe (PR-EX-TnIR-A-10) was used to reduce artifacts from silicon IR absorption, allowing operation in both CM and TM modes. In the 4000–2700 cm⁻¹ range, CM was employed with the “pure contact” model (PR-EX-nIR2-1).

2.5. NanoSIMS

C, N and H isotopic measurements of C0052 particle were performed with the Cameca NanoSIMS 50 ion microprobe instrument at Wash U in St. Louis. The samples were measured in two sessions using a ~2.7–3.5 pA Cs⁺ primary beam focused to 100 nm. In the first session, we collected ¹²C⁻, ¹³C⁻, ¹²C¹⁴N⁻, ¹²C¹⁵N⁻ and ²⁸Si⁻ for C and N isotopes. In the second session, we collected H⁻ and D⁻ for H isotopes. Before measurement, the analyzed areas were pre-sputtered on an 8×8 μm² area for ~500 s. Then, the primary beam was rastered over a 5×5 μm area, divided into 256×256 pixels. For C and N isotopes, the mass resolving power (MRP) was set to ~5700 to resolve ¹²CH⁻ and ¹³C¹⁴N⁻ interferences on ¹³C and ¹²C¹⁵N⁻, respectively. For H isotopes, the MRP was set to ~1700. We used a kerogen standard (pressed into copper stub) from Chert (Warrawoona Group, Australia, 3.5 billion years) containing 64 wt.% of C, with an wt.% C/N ratio of 181.59, H/C ratio of 0.3, δ¹³C_{PDB} of -34.3 ‰, δ¹⁵N_{AIR} of 5.5 ‰ (Beaumont and Robert, 1999), and δD_{SMOW} = -105.3‰ as reference material to correct for instrumental mass fractionation (IMF). The IMF was on the order of $-111 \pm 7\text{‰}$ (1σ) for C, $-163 \pm 13\text{‰}$ for N, and $-120 \pm 108\text{‰}$ for H (Figure S6). We collected a total of 30 cycles and manually removed cycles until counts are stable. We typically achieved a counting statistic of $\leq 4\text{‰}$ for δ¹³C, $\leq 40\text{‰}$ for δ¹⁵N and $\leq 30\text{‰}$ for δD on kerogen. The NanoSIMS image data were processed using an in-house MATLAB code and corrected for the deadtime, and quasi-simultaneous arrival (QSA) effects following the method described by Ogliore et al. (2021) (see supplementary material S5). NanoSIMS image frames were aligned to correct for stage or beam drift. Pixels

from $\delta^{13}\text{C}$, $\delta^{15}\text{N}$, and δD images were resized so that the pixel size was larger than the beam size. C, N and H isotopic ratios ($^{13}\text{C}/^{12}\text{C}$, $^{15}\text{N}/^{14}\text{N}$ and D/H) are reported as delta values, relative to PDB ($\delta^{13}\text{C}_{\text{PDB}} = (^{13}\text{C}/^{12}\text{C})_{\text{sample}}/(^{13}\text{C}/^{12}\text{C})_{\text{PDB}} - 1] \times 1000$, PDB = Pee Dee Belemnite), AIR ($\delta^{15}\text{N}_{\text{AIR}} = (^{15}\text{N}/^{14}\text{N})_{\text{sample}}/(^{15}\text{N}/^{14}\text{N})_{\text{AIR}} - 1] \times 1000$), and SMOW ($\delta\text{D}_{\text{SMOW}} = [(\text{D}/\text{H})_{\text{sample}}/(\text{D}/\text{H})_{\text{SMOW}} - 1] \times 1000$, SMOW = Standard Mean Ocean Water), respectively.

3. Results

3.1. Reflectance spectroscopy

The IR reflectance spectra of particles C0050 and C0052, acquired under N_2 in the wavelength range from 2 μm to 4 μm , are shown in Figure 1. These spectra can be compared to the MicrOmega spectra acquired inside the curation facility¹, the spectrum of Ryugu bulk samples from Chamber C (Yada et al., 2021), and the CI chondrite Orgueil (Potin et al., 2020). The spectra of particles C0050 and C0052 exhibit a prominent absorption band at $\sim 2.7 \mu\text{m}$, due to hydroxyl ($-\text{OH}$) in phyllosilicates (T. Nakamura et al., 2022). This observation is consistent with the FTIR spectra obtained from the bulk Ryugu samples from Chamber C (Yada et al., 2021), the CI Orgueil and other hydrated carbonaceous chondrites (Potin et al., 2020; Amano et al., 2023). However, our reflectance spectra show a broader absorption feature between $\sim 2.7 \mu\text{m}$ to $3 \mu\text{m}$ compared to the MicrOmega spectra acquired in JAXA's curation facility, suggesting a slight absorption of molecular water despite our precautions during sample handling and storage. In addition, no other spectral features such as those of organic molecules (3.4 μm and 3.5 μm) and carbonate (3.4 μm and 3.9 μm) are visible on our spectra.

Notably, the MicrOmega and IPAG spectra of particles C0050 and C0052 shown in Figure 1 do not have absorption feature around 3.06 μm and 3.24 μm that could be attributed to NH/NH_4^+ -bearing compounds, although the FTIR spectra on which we based our grain selection show absorptions around these wavelengths (Figure S1). Since both FTIR and MicrOmega instruments operate within JAXA's curation facility, the differences between their spectra of the same grains are either due to instrumental artefact(s) of the FTIR measurement (possibly due to a water ice film on the detector, as mentioned in Hatakeyama et al. (2023)) and/or to a change of the rain composition between the FTIR and MicrOmega measurements (potentially due to a loss of volatile compounds due to the vacuum tweezer used to manipulate the grains within the facility, and/or due to heating of these extremely dark grains during their illumination). Since the spectra measured outside the curation facility resemble the MicrOmega spectra, we favor the first hypothesis, although the second one might not be totally excluded.

¹The MicrOmega spectra were available from the Ryugu Sample Data System after the first AO allocation deadline. Therefore, our grain selection was only based on the FTIR spectra.

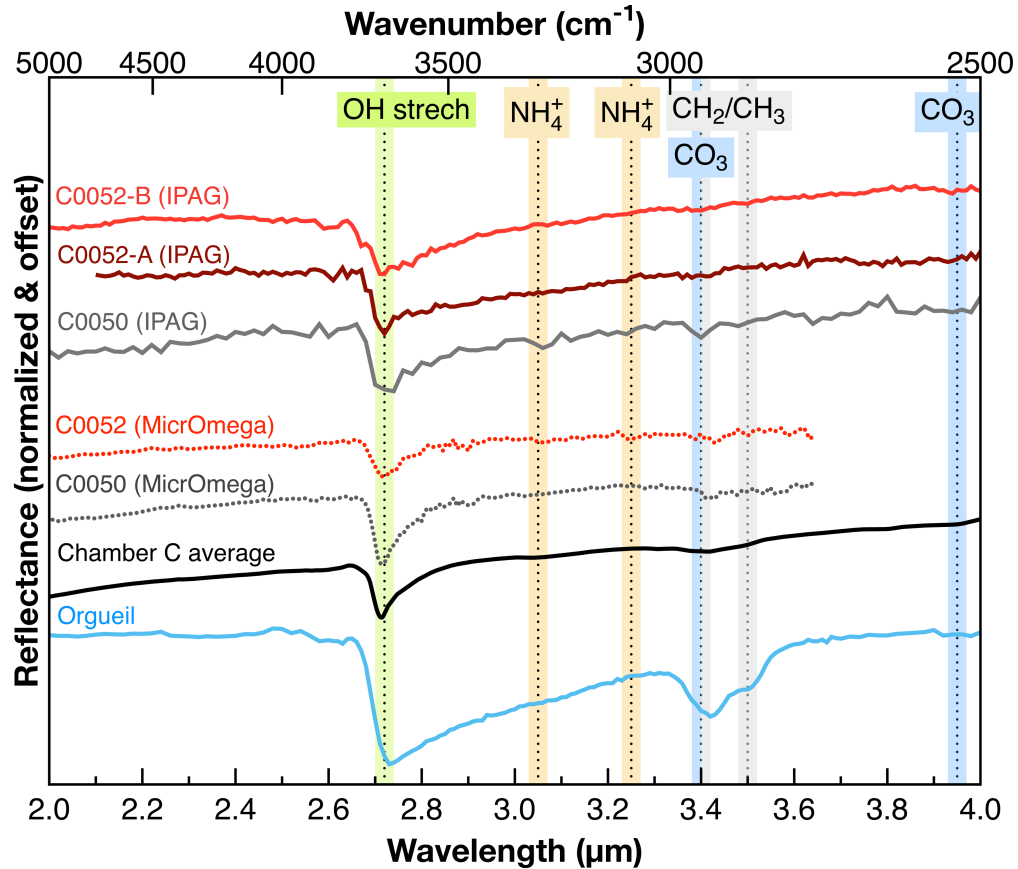


Figure 1. Reflectance spectra between 2 μm to 4 μm (normalized to 2.5 μm) of Ryugu particles C0052 (red) and C0050 (grey), compared to MicrOmega measurements (dotted spectra), averaged Ryugu samples from Chamber C (solid black spectrum, Yada et al. 2022), and the CI chondrite Orgueil (solid blue spectrum, Potin et al., 2020). The particle C0052 has been analyzed on both sides up and down (C0052-A and B). Typical OH (2.7 μm , in green), NH₄⁺ (3.05 μm and 3.25 μm , in yellow), organic molecules (3.4 μm and 3.5 μm , in grey), and carbonate (3.4 μm and 3.9 μm , in blue) band positions are highlighted by vertical black dotted lines.

3.2. Transmission spectroscopy

The μ -FTIR spectra of crushed fragments from particles C0050 and C0052, obtained under N_2 and atmospheric conditions, are depicted in Figure 2. The spectra acquired under N_2 display homogeneity, with consistent peak positions and shapes indicating the presence of various compounds, such as Mg-rich phyllosilicates (notably --OH stretching at $\sim 3690 \text{ cm}^{-1}$ and Si-O stretching at $\sim 1000 \text{ cm}^{-1}$), organic compounds (including CH_2 and CH_3 stretching modes at $\sim 2950\text{--}2860 \text{ cm}^{-1}$, and double bond $\text{C}=\text{C}$ at $\sim 1600 \text{ cm}^{-1}$ for C0050, respectively), and possibly minor contribution from carbonates (CO_3 bending et in-plane modes at $\sim 1450 \text{ cm}^{-1}$ and 880 cm^{-1}). These IR signatures are similar to those previously measured in other Ryugu particles (Dartois et al., 2023; Phan et al., 2024; Bonal et al., 2024; Yesiltas et al., 2024; Quirico et al., 2024) and CI chondrites, such as Orgueil and Ivuna (Beck et al., 2010).

The IR spectra acquired under atmospheric conditions are similar to those obtained under N_2 , but exhibit additional features, including a broad O-H stretching band at $\sim 3400 \text{ cm}^{-1}$ and a H-O-H bending band at $\sim 1650 \text{ cm}^{-1}$. These bands are less prominent in samples analyzed under N_2 environment and are attributed to water molecules loosely adsorbed to minerals and as interlayer molecular water in phyllosilicates due to terrestrial contamination. In some spectra obtained from particle C0052 (Figure S3), we also observed a broad band at $\sim 3250 \text{ cm}^{-1}$ (7-G2-1 and 7-G1-3 from Figures 2 and S3). This spectral signature overlaps with the main asymmetric stretching vibration mode of NH_4^+ ($\sim 3250 \text{ cm}^{-1}$; Fastelli et al. 2020; Petit et al. 2006), but it also matches the vibration mode of water ice at $\sim 3000\text{--}3200 \text{ cm}^{-1}$ (depending on the temperature), which may have condensed on the liquid-nitrogen-cooled detector of the FTIR microscope during analysis (Hatakeyama et al., 2023). Although we carefully collected and subtracted each background before collecting the spectrum of the sample to minimize the appearance of a water ice signal, we cannot exclude the possibility that this broad band is caused solely by this instrumental artifact.

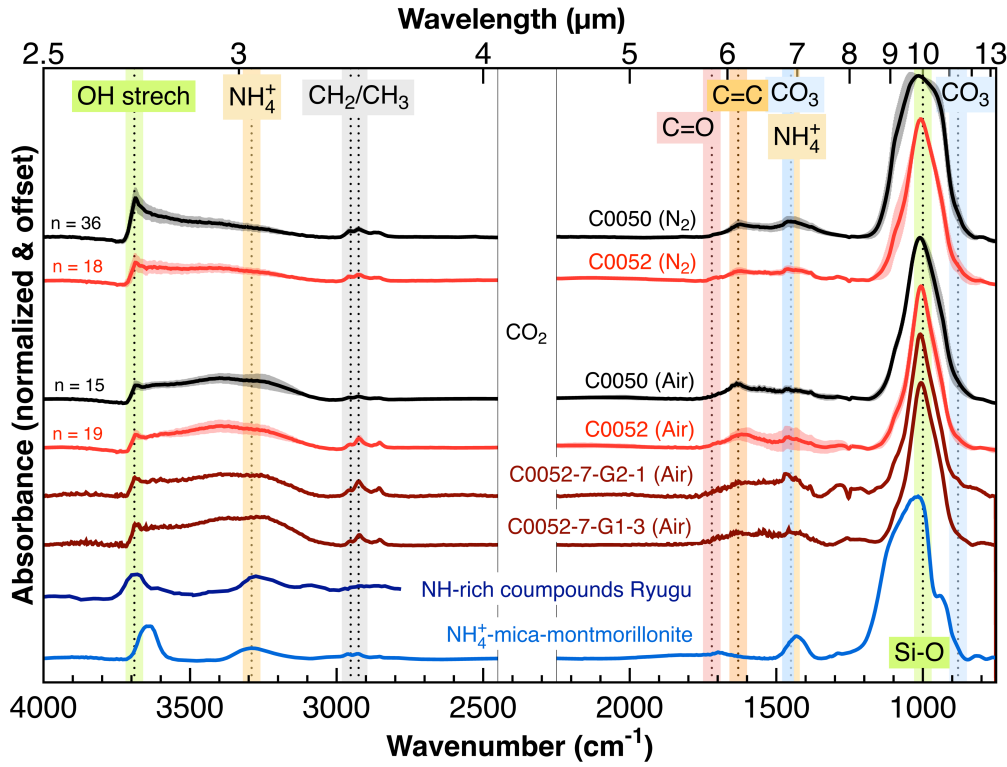


Figure 2. μ -FTIR spectra (normalized to 1000 cm^{-1}) of multiple crushed grains extracted from particles C0050 and C0052, collected under N_2 or air conditions. All spectra were averaged for each particle acquired under the same conditions, with their 1σ error indicated by the shaded area. The spectra of specific regions in particle C0052 (7-G2-1 and 7-G1-3), showing a broad band at $\sim 3250\text{ cm}^{-1}$ corresponding possibly to the vibration mode of NH_4^+ , an NH-rich grain in bulk Ryugu (Pilorget et al., 2022), and an NH_4^+ -mica-montmorillonite (Phan et al., 2022) reference material are shown individually for comparison. The peaks at 2360 cm^{-1} corresponding to atmospheric CO_2 are hidden for clarity. Colored dashed lines represent identified bands: green for phyllosilicate OH (3690 cm^{-1}) and Si-O bands (1000 cm^{-1}), yellow for NH_4^+ bands (3250 cm^{-1} and 1450 cm^{-1}), gray for aliphatic C-H bands (2960 cm^{-1} for CH_3 asymmetric stretching and 2925 cm^{-1} for CH_2 symmetric stretching), red for the carbonyl (C=O) band (1720 cm^{-1}), orange for the aromatic ($\text{C}=\text{C}$) band with some contribution from water bending modes ($\sim 1600\text{ cm}^{-1}$), and blue for carbonate (CO_3) bands (1440 cm^{-1} and 880 cm^{-1}).

3.3. AFM-IR Imaging and Spectroscopy

Using the Tapping IR mode, we investigated the spatial distribution of different functional groups with IR signatures across the entire surface of the C0050 and C0052. A $5 \times 5 \mu\text{m}$ ROI of C0052 was recorded with a higher spatial resolution of 500×500 points (obtaining theoretical spatial resolution imaging of $\sim 10 \text{ nm}$) (Figure 3a) (Phan et al., 2022). AFM-IR images obtained at various wavenumbers reveal the distribution of different absorptions: 1660 cm^{-1} (red), 1550 cm^{-1} (yellow), and 1450 cm^{-1} (blue) attributed to CH_2 bending or $\text{CO}_3^{2-}/\text{NH}_4^+$ bending mode, and phyllosilicate (Si-O) at 1000 cm^{-1} (green, Figure 3b–e). Figures 3f and 3g display two composite RGB images, showing IR intensities at 1660 cm^{-1} , 1550 cm^{-1} , and 1000 cm^{-1} (Figure 3f), and at 1660 cm^{-1} , 1450 cm^{-1} , and 1000 cm^{-1} (Figure 3g). These maps, along with AFM-IR spectra from $2000\text{--}700 \text{ cm}^{-1}$, reveal three domains: (i) a prominent Si-O stretching band around 1000 cm^{-1} in phyllosilicates (green areas in Figures 3e–g), (ii) strong absorption peaks at 1660 cm^{-1} and 1550 cm^{-1} , unusual for OM found in meteorites or Ryugu sample (Phan et al., 2022; Phan et al., 2024; Mathurin et al., 2024) and (iii) small blue regions (Figure 3d) suggesting either CH_2 bending indicative of aliphatic organic compounds, or carbonates.

To gain more detailed insights, we obtained numerous single-point AFM-IR spectra in the $2000\text{--}700 \text{ cm}^{-1}$ range. The average B spectrum ($n = 48$) shows a strong 1000 cm^{-1} peak typical of phyllosilicates in Ryugu (Figure 3). The C spectrum shows two distinct yet concurrent peaks at 1450 cm^{-1} and 880 cm^{-1} , predominantly associated with the bending and in-plane formation modes characteristic of carbonate minerals, such as dolomite and/or calcite (Phan et al., 2022, 2024). Five spectra from the orange and pink areas (A1–A5) show peaks at 1660 cm^{-1} and 1550 cm^{-1} , distinct from the typical OM in Ryugu particles (Phan et al., 2024). The position and relative intensity of these two peaks are commonly attributed to the amide group (e.g., $-\text{C}(=\text{O})\text{-NH-}$), with the peak at 1660 cm^{-1} mainly due to C=O stretching (so-called “amide I” band) and 1550 cm^{-1} mainly due to N-H bending vibration mode (so-called “amide II” band). SEM-EDS data indicate that these organic-rich regions are enriched in N in comparison to the surrounding areas (Figure S2). A similar spectral signature was also found in another area in the 7-G1-3 grain, showing double peaks at 1660 cm^{-1} and 1550 cm^{-1} (Figure S4).

The 7-G2-1 region was also analyzed in CM using the FF laser ($3800\text{--}2700 \text{ cm}^{-1}$ range) across areas with and without amides (Figure S5). This analysis revealed a significant contribution from $-\text{OH}$ stretching at 3680 cm^{-1} and strong absorption at 2930 cm^{-1} and 2960 cm^{-1} , highlighting aliphatic asymmetric stretching modes in OM. The aliphatic signatures were more pronounced in the region associated with amides compared to those associated with phyllosilicates. Peaks in the range of 3358 cm^{-1} to 3240 cm^{-1} were detected in the region associated with amides, possibly corresponding to the characteristic N-H stretching mode of amide A (Ji et al., 2020). However, it remains unclear whether these peaks definitively

correspond to N-H stretching of amide due to the low signal-to-noise ratio and potential physical damage to the AFM tips during IR mapping in CM.

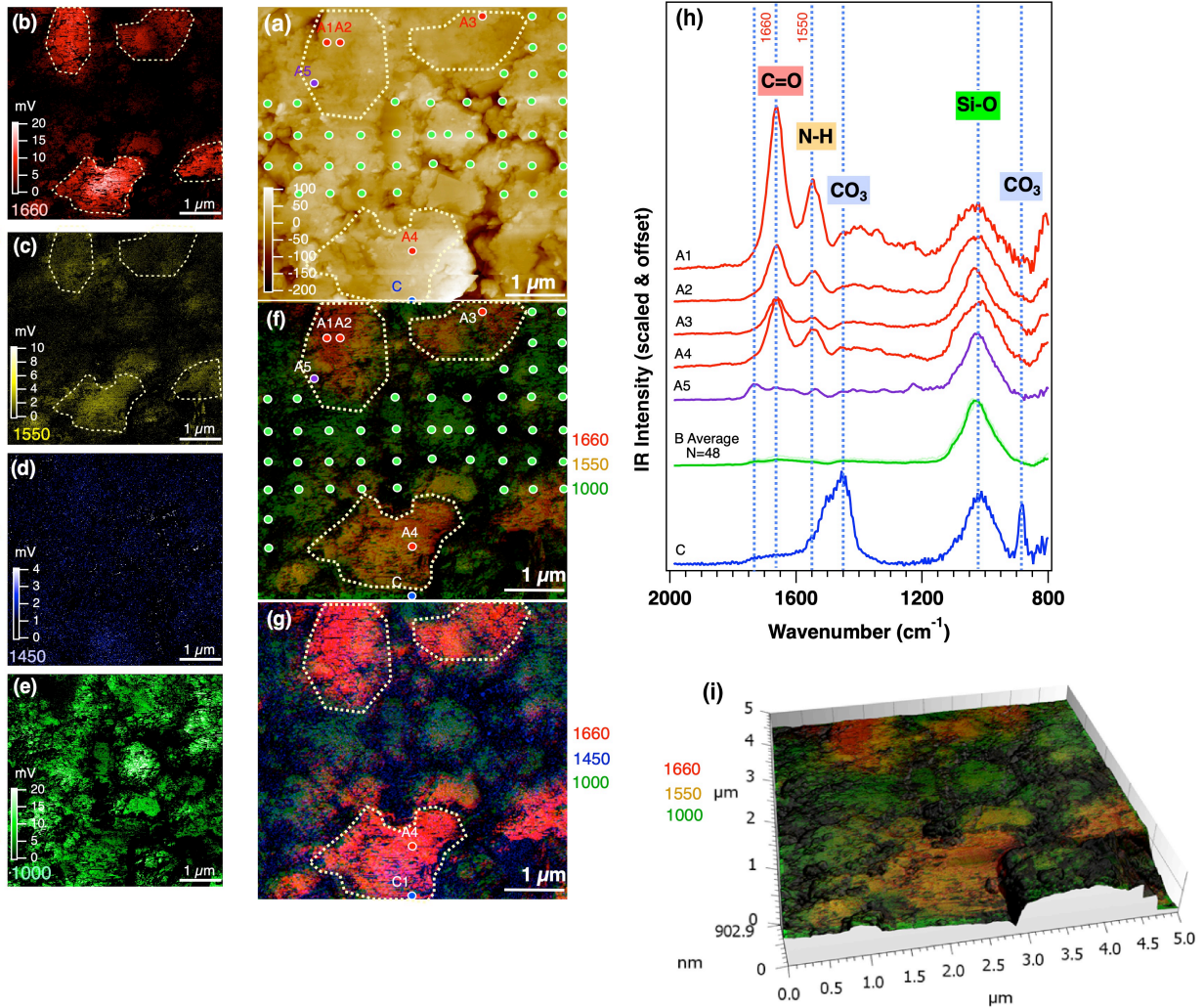


Figure 3. AFM-IR tapping IR maps using the APE laser ($2000\text{-}700\text{ cm}^{-1}$) of the 7-G2-1 region with (a) AFM image from particle C0052 at spectral bands of (b) 1660 cm^{-1} and (c) 1550 cm^{-1} (C=O from organic matter and C=O from amide group and H₂O); (d) 1450 cm^{-1} (carbonate bending mode or ammonium); and (e) 1000 cm^{-1} (phylllosilicates); and combined (f) RGY and (g) RGB maps ($R = 1660\text{ cm}^{-1}$; $G = 1000\text{ cm}^{-1}$, $Y = 1550\text{ cm}^{-1}$, $B = 1450\text{ cm}^{-1}$). The organic-rich region is highlighted by white dashed lines. (h) AFM-IR contact spectra associated with different positions located in the AFM topographic map. AFM-IR spectra of A1-A4 show double peaks at $\sim 1660\text{ cm}^{-1}$ and $\sim 1550\text{ cm}^{-1}$ possibly related to C=O stretching and -NH bending vibration mode of amide group (-C(=O)-NH-), respectively. The vertical blue dashed lines highlight the characteristic band positions of C=O and N-H from the amide group at 1660 and 1550 cm^{-1} (black), NH₄⁺ at 1450 cm^{-1} (yellow), phylllosilicates at 1000 cm^{-1} (green), and carbonates (CO₃) at 1440 and 880 cm^{-1} (blue). (i) composite 3-D view of the RGY image derived from the three maps: 1660 cm^{-1} , 1000 cm^{-1} , and 1550 cm^{-1} , respectively, showing the areas containing the amides.

3.4. NanoSIMS

High spatial resolution NanoSIMS mapping ($5 \times 5 \mu\text{m}^2$ of 256×256 pixels) was conducted on the same area where N-H organic compounds were detected by AFM-IR (Figure 3), and in surrounding areas. In the first session, we collected $^{12}\text{C}^-$, $^{13}\text{C}^-$, $^{12}\text{C}^{14}\text{N}^-$, and $^{12}\text{C}^{15}\text{N}^-$ ions to determine their respective $\delta^{13}\text{C}$ and $\delta^{15}\text{N}$ values. Using AFM-IR tapping mode map at 1660 cm^{-1} and NanoSIMS accumulated images of $^{12}\text{C}^{14}\text{N}^-$ ions as reference images, we defined ROIs on the corresponding NanoSIMS images to select only pixels from the N-H organic compound areas (Figure 4, Table 1). Given that our NanoSIMS investigations were focused solely on the 7-G2-1 area (where AFM-IR detected the amides), we inferred that the $^{12}\text{C}^{14}\text{N}^-$ -rich regions in the surrounding areas, which display similar $^{12}\text{C}^{14}\text{N}^-$ counts per pixel and $^{12}\text{C}^{14}\text{N}^-/^{12}\text{C}^-$ ratios (Table 1), correspond to the same N-H organic compounds observed in Figure 3 (Figures S6–S7).

The C isotopic compositions of the amides are within the range of terrestrial values, with $\delta^{13}\text{C}$ values ranging from $-69 \pm 66 \text{ ‰}$ to $0 \pm 29 \text{ ‰}$ (2σ), with a weighted mean of $-26 \pm 63 \text{ ‰}$ (2σ , $n = 6$). In contrast, their N isotopic compositions are highly depleted in ^{15}N , with $\delta^{15}\text{N}$ values ranging from approximately $-307 \pm 52 \text{ ‰}$ to $-123 \pm 34 \text{ ‰}$, yielding a weighted mean of $-213 \pm 103 \text{ ‰}$ ($n = 8$). Their associated $^{12}\text{C}^{14}\text{N}^-/^{12}\text{C}^-$ ratios (used to approximate their wt.% N/C ratio) indicate that these organic compounds are enriched in N compared to their surrounding matrix, with $^{12}\text{C}^{14}\text{N}^-/^{12}\text{C}^-$ ratios between 0.106 and 0.149, averaging 0.133 ± 0.031 ($n = 6$, Table 1).

In the second session, we collected $^1\text{H}^-$ and D ions to estimate the δD values of the same ROIs defined during the first session. Following the C and N analysis, and due to sample consumption, we relied on secondary electron (SE), $^{12}\text{C}^{14}\text{N}^-$, and $^1\text{H}^-$ images to identify the remaining N-H organic compounds and establish ROIs for H isotope analysis (Figures 4 and S7). Although we systematically compared the last cycle of $^{12}\text{C}^{14}\text{N}^-$ with the first cycle of $^1\text{H}^-$ images to locate the remaining N-H organic compounds based on their shape and size, we cannot exclude the possibility that some amide grains may have been completely consumed in some of the analyses after the C and N measurements. Nevertheless, the H isotopic compositions of the expected NH-rich regions are not anomalous in D compared to terrestrial values, with δD values ranging from $-121 \pm 277 \text{ ‰}$ to $429 \pm 344 \text{ ‰}$ (2σ), with a weighted mean of $194 \pm 368 \text{ ‰}$ ($n = 7$, Table 1).

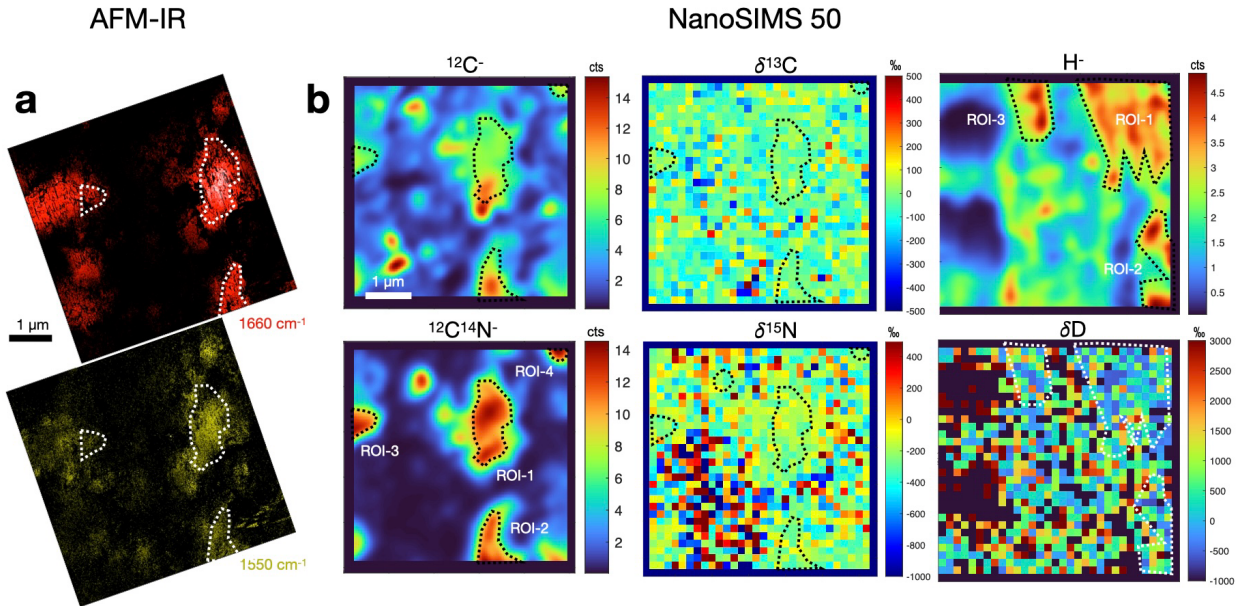


Figure 4. Combined AFM-IR and NanoSIMS high resolution spatial analyses of N-H organic compounds. (a) AFM image of the 7-G2 region from particle C0052 at spectral bands of 1660 cm^{-1} (C=O from organic matter) and 1550 cm^{-1} ($-\text{NH}$ bending vibration mode of amide group). (b) Corresponding NanoSIMS accumulated images ($5 \times 5 \mu\text{m}^2$) of $^{12}\text{C}^-$, $^{12}\text{C}^{14}\text{N}^-$ and $^1\text{H}^-$ ions, $\delta^{13}\text{C}$, $\delta^{15}\text{N}$ and δD . The ROIs used to extract pixels only from the NH-rich regions detected by AFM-IR are outlined by black or white dashed lines. ROIs shapes between $^{12}\text{C}^-$ – $^{12}\text{C}^{14}\text{N}^-$ and $^1\text{H}^-$ NanoSIMS images are different due to sample consumption between the two analytical sessions (Figure S7).

Table 1 - C, N and H isotopic composition of the amides determined by NanoSIMS.

Sample	ROI size (μm^2)	^{12}C (c/px)	$\delta^{13}\text{C}$ (‰)	2σ	$^{12}\text{C}^{14}\text{N}$ (c/px)	$\delta^{15}\text{N}$ (‰)	2σ	$^{12}\text{C}^{14}\text{N}/^{12}\text{C}$	ROI size (μm^2)	^1H (c/px)	δD (‰)	2σ
ROI-1	1.12	527	0	29	748	-198	38	0.127	2.83	219	190	245
ROI-2	0.49	602	-7	33	716	-218	50	0.106	0.44	236	130	363
ROI-3	0.2	453	-3	47	758	-227	70	0.149	0.55	238	390	319
ROI-4	0.08	530	-69	66	860	-215	100	0.145	n.a.			
ROI-5	1.03	—	—	—	1131	-123	34	—	1.27	146	121	308
ROI-6	0.25	—	—	—	1198	-147	51	—	0.54	182	429	344
ROI-7	1.48	535	-34	28	820	-237	35	0.137	1.90	198	-121	277
ROI-8	0.92	260	-6	35	396	-307	52	0.136	0.48	466	159	291
Weighted mean		485	-26		828	-213	0.133			214	194	
2σ		239	63		502	103	0.031			209	368	

Note. “—” denotes discarded values; “n.a.” = not analyzed.

4. Discussion

4.1. Detection and identification N-H organic compounds in Ryugu and CI chondrites

Confirmed N-H absorption bands have been previously reported in a few bulk Ryugu particles by Pilorget et al. (2022) and Yada et al. (2022). Jiang et al. (2024), analyzed numerous Ryugu grains at JAXA curation using MicrOmega, identifying only rare regions, a few hundred μm in size, with a prominent $\sim 3.06 \mu\text{m}$ absorption feature, indicative of NH-bearing compounds. This spectral signature likely corresponds to NH_4^+ and/or other NH-bearing organic molecules such as amines ($\text{R}-\text{NH}_2$) detected in Ryugu A0106 and C0107 particles through hot water extractions, and hypothesized to be mainly in the form of salts (Naraoka et al., 2023; Yoshimura et al., 2023; Takano et al., 2024).

Here, we report the detection of amides ($-\text{C}(=\text{O})-\text{NH}$ -bearing organic compounds) at sub-micrometer-scale by AFM-IR (Figure 3), in locations of Ryugu grains where the N-H absorption band was also detected at micrometer-scale by μ -FTIR (Figure 2). In total, we analyzed $\sim 7380 \mu\text{m}^2$ of surface area across the C0050 and C0052 Ryugu particles using AFM-IR and detected amide-related organic compounds in only $\sim 35 \mu\text{m}^2$ (Tables S1 and S2), representing $\sim 1 \text{ vol.}\%$ of the total analyzed surface. This result suggests that amides are relatively rare in our Ryugu samples and are heterogeneously distributed on a micrometer scale. Therefore, amides are likely contributors to the $\sim 3.06 \mu\text{m}$ absorption feature (via their amide A band), together with NH_4^+ and amines.

In meteorites, amide-related organic compounds have been previously reported in aqueously altered carbonaceous chondrites. The quantities of amino acids and amines extracted from carbonaceous chondrites generally increase by a factor of two, and sometimes much more (up to about 10), when an acid hydrolysis is performed following, or instead of, a water extraction. Therefore, a significant fraction of these molecules is initially in the form of acid-labile precursors, such peptide-like structures and amides (Cronin, 1976a; Pizzarelli and Holmes, 2009; Burton et al., 2014; Aponte et al., 2014; Kebukawa et al., 2019a; Glavin et al., 2020). Such increases of amino acid yields after acid hydrolysis were also observed on lunar regolith samples, and potentially attributed to precursors contained in meteorites, micrometeorites, or inter-planetary dust particles (Elsila et al., 2016). Analyses performed so far on the A0106 and C0107 Ryugu grains revealed that most amino acids were extracted in hot water, without acid hydrolysis. A notable exception is γ -amino-n-butyric acid whose abundance increased by a factor of more than 15 after acid hydrolysis, indicating that it is present in the form of precursors possibly including the amides γ -lactams (Parker et al., 2023).

Several studies have investigated acid-labile amino acid precursors in carbonaceous chondrites, particularly in the CM2 Murchison, highlighting diverse molecular origins. Acid hydrolysis has been shown to convert amides, including aliphatic amides in Murchison and polymer amides in both Murchison and CV3 Allende, into amino acids (Cronin, 1976a, b; Cooper and Cronin, 1995; McGeoch and McGeoch,

2015). Meierhenrich et al. (2004) reported higher concentrations of diamino acids in Murchison after acid hydrolysis compared to water extraction, suggesting these compounds originally existed as higher-molecular-mass precursors. Shimoyama and Ogasawara (2002) detected the presence of dipeptide (glycyl-glycine) in Murchison and CM2 Yamato-791198, while Lange et al. (2020) found that most amino acids in acid-hydrolyzed meteorite extracts originate from non-peptide precursors, though they confirmed the presence of peptide sequences in Murchison. In Ryugu samples, while numerous N-bearing organic molecules, such as N-heterocycles, amines, hydroxy compounds, and N-heterocyclic indoles, have been identified via hot water extraction (Naraoka et al., 2023; Oba et al., 2023; Takano et al., 2024). However, amides or polypeptides acid-labile precursors have yet to be recovered from Ryugu samples.

FTIR analysis of the acidic residues from Ryugu particles, however, revealed two distinct phases: one resembling the insoluble organic matter (IOM) typical of unheated carbonaceous chondrites type 1 and 2 (Kebukawa et al., 2011; Orthous-Daunay et al., 2013; Quirico et al., 2023), and the other representing an “outlier phase” (Kebukawa et al., 2024). Notably, a peak at 1660 cm^{-1} , attributed to C=O stretching in amide compounds ($\text{R}-(\text{C=O})-\text{N}-\text{H}-\text{R}'$) or unsaturated ketones/aldehydes, was consistently observed in residues C0107, A0106, and C0002 (Kebukawa et al., 2024) (Figure 5). Furthermore, two absorption bands at 3350 cm^{-1} and 3180 cm^{-1} were detected in the “outlier phase” of residues A0106 and C0107, likely corresponding to N-H stretching. Interestingly, the peak at 1550 cm^{-1} , commonly associated with N-H bending in amide compounds, was absent in all spectra of these residues (Kebukawa et al., 2024). This outlier phase was exclusively observed in the acid residues of C0107, A0106, and C0002 which was extracted using HF/HCl demineralization and following solvent extraction protocols, as described by Yabuta et al. (2023) and Naraoka et al. (2023). In contrast, this outlier phase was not observed in acid residues prepared by Quirico et al. (2023), including A0106, which were obtained using a different HF/HCl protocol (Orthous-Daunay et al., 2010). This discrepancy could be attributed to sample heterogeneities (Kebukawa et al., 2024), especially given the small sample amount used by Quirico et al. (2023) compared to Yabuta et al. (2023). However, the possibility of contamination cannot be ruled out. Kebukawa et al. (2024) demonstrated that the infrared spectra of very simple molecules closely match the spectrum of this outlier phase. This finding is somewhat unexpected, given the broad diversity of organic species in soluble organic matter (SOM) (Schmitt-Kopplin et al., 2023) and the observed decrease in abundance with increasing carbon chain length (Kebukawa et al., 2024).

The faint absorption band around $3.06\text{ }\mu\text{m}$, attributed to NH-rich compounds, observed in spectral average of several Ryugu grains within the curation facility (Pilorget et al., 2022; Yada et al., 2022), is not observed here in mm-scale spectra of the bulk C0050 and C0052 particles (Figure 1), most probably because the width of the $2.7\text{-}\mu\text{m}$ absorption band extends up to more than $3.1\text{ }\mu\text{m}$ because of the adsorption of water

molecules, thus masking any faint absorption potentially present. However, absorption around $\sim 3250\text{ cm}^{-1}$ was observed locally at μm -scale, on crushed fragments of these grains (Figure 2).

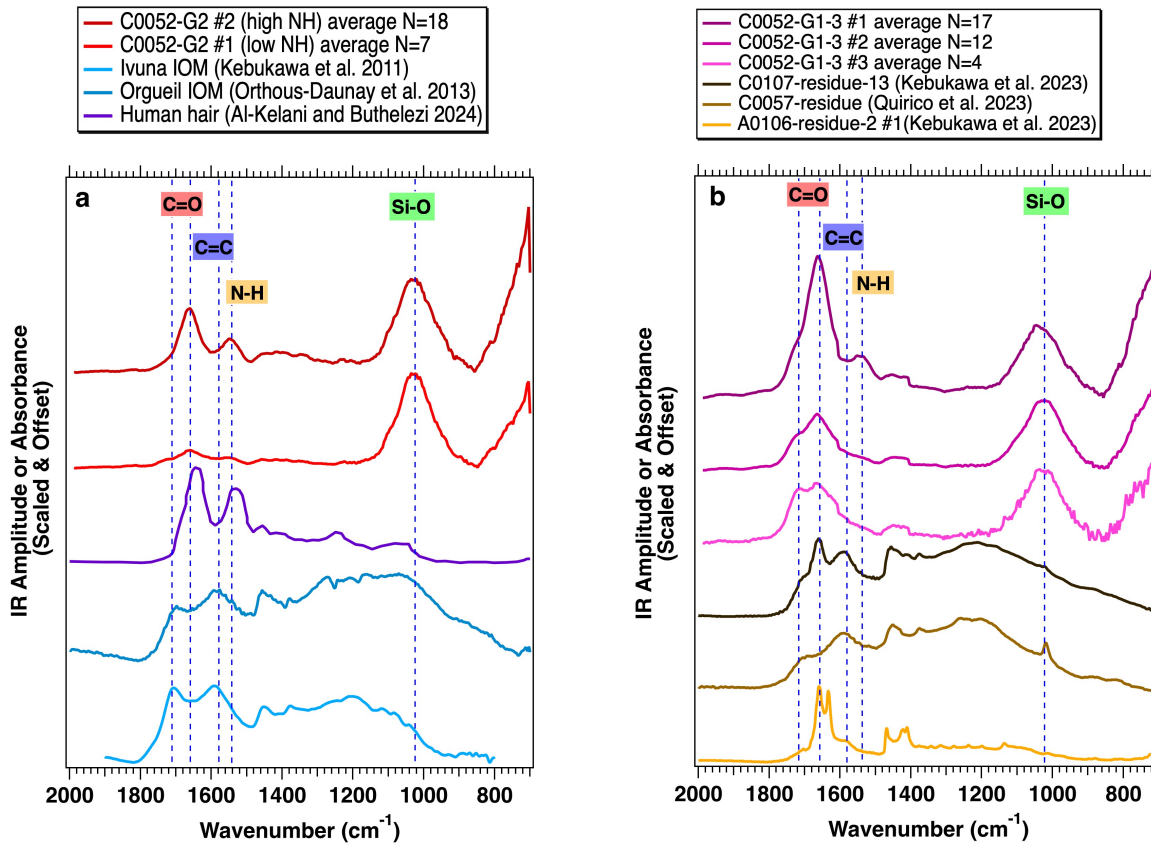


Figure 5. AFM-IR spectra of Ryugu grains C0052: (a) 7-G2 and (b) 7-G3 showing key vibrational bands for C=O, C=C, N-H, and Si-O (indicated by blue dashed lines). For comparison, the IR spectra of Ivuna IOM (Kebukawa et al., 2011), Orgueil IOM (Orthous-Daunay et al., 2013), and human hair (Al-Kelani and Buthelezi, 2024) are included, along with acid residues from Ryugu samples C0057 (Quirico et al., 2023), A0106, and C0107 (Kebukawa et al., 2024). Spectra are scaled and offset for clarity.

4.2 Potential source of contaminations

Given that the amides were detected solely in a single preparation of C0052 (Figure S3), one possibility is that this phase resulted from terrestrial contamination either before shipment to our laboratory or during sample preparation and/or IR measurements. Concerning the former, Kebukawa et al. (2024) discussed possible contamination sources in Ryugu samples, including artificial OM particles inside sample containers at the JAXA Curation Center (Yada et al., 2014; Uesugi et al., 2014) or explosives contaminants introduced during FTIR measurements (Takano et al., 2020; Ito et al., 2021). However, a comparison of these potential contaminants with the spectra from the C0052 grain reveals no spectral match with the amide phases identified in C0052 through AFM-IR analysis.

Another possibility of contamination is during sample preparation and measurements in our laboratory. Contamination from human skin or hair, for example, could have been introduced during sample handling. Kebukawa et al. (2024) provided an IR spectrum extracted from human skins treated with HF/HCl, and FTIR spectra of untreated human skin or hair are available in the literature (Wang et al., 2012; Al-Kelani and Buthelezi, 2024) (Figure 5a). The two peaks at 1645 cm^{-1} and 1530 cm^{-1} from the human hair are fairly consistent with the amide phase in Ryugu C0052 (1660 cm^{-1} and 1550 cm^{-1}), which could suggest a contamination origin. However, the N isotopic composition of the amides in Ryugu C0052 is significantly depleted in ^{15}N ($\delta^{15}\text{N} = -215 \pm 92\text{ ‰}$, Table 1) compared to human hair samples, which have a bulk $\delta^{15}\text{N}$ of $\sim 10\text{ ‰}$ (Petzke et al., 2005). These isotopic differences strongly suggest that the amide phase in Ryugu C0052 grains is indigenous to the samples, rather than the result of a laboratory contamination.

4.3 Possible Mechanisms for the Formation of Amides in Ryugu Samples

4.3.1 Hydrothermal condition on the Ryugu's parent planetesimal?

Abiotic formation of amides is feasible under low-temperature hydrothermal conditions (≤ 300 °C) through condensation of carboxylic acids with $\text{NH}_3/\text{NH}_4^+$ or amines, followed by dehydration (Figure 6) (Rushdi and Simoneit, 2004; Lange et al., 2020; Fu et al., 2020; Kebukawa et al., 2024; Serra et al., 2024). Indeed, carboxylic acids, NH_4^+ , and aliphatic amines have been detected in Ryugu samples and carbonaceous chondrites, particularly in hot water extracts (Sephton, 2002; Naraoka et al., 2023; Yoshimura et al., 2023; Schmitt-Kopplin et al., 2023; Takano et al., 2024). The presence of these compounds, along with evidence of extensive aqueous alteration on Ryugu's parent asteroid, supports the hypothesis that amides in Ryugu could form via hydrothermal alteration (Kebukawa et al., 2024).

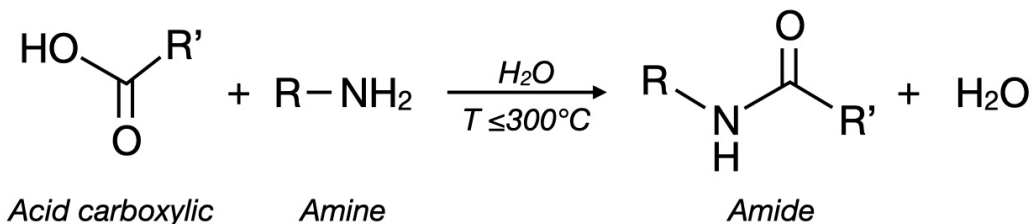


Figure 6 - Hydrothermal formation of amides through condensation of amines and carboxylic acids. (adapted from Fu et al., 2020). R and R' represent generic alkyl or aromatic groups.

Assuming the amides in Ryugu formed through the condensation of carboxylic acids and amines/ NH_4^+ , their N, C, and H isotopic signatures should approximately align with those of their expected precursor molecules (Marlier et al., 1999). Takano et al. (2024) reported the C and N isotopic compositions of water-soluble organic molecules (WSOM) extracted from Ryugu samples, including carboxylic acids and amines. Their $\delta^{13}\text{C}$ values were consistent within error ($\delta^{13}\text{C} = -26\text{ ‰}$ to -20 ‰) with the amide phase observed in this study (Figure 7a). However, their $\delta^{15}\text{N}$ values ($\delta^{15}\text{N} = -3\text{ ‰}$ to 63 ‰) were significantly enriched in ^{15}N when compared to the extremely depleted $\delta^{15}\text{N}$ value of the amide phase in Ryugu ($\delta^{15}\text{N} = -215 \pm 92\text{ ‰}$, Figure 7a, Table 1).

Additionally, Becker and Epstein (1982) measured δD values from the SOM in various carbonaceous chondrites ($\delta\text{D} = -46\text{ ‰}$ to 486 ‰ , Figure 7b), showing ranges comparable to those of Ryugu's amide phase ($\delta\text{D} = 194 \pm 368\text{ ‰}$). Despite similar $\delta^{13}\text{C}$ and δD values, the $\delta^{15}\text{N}$ of the amides in Ryugu are strikingly depleted in ^{15}N compared to the WSOM and SOM from both Ryugu and carbonaceous chondrites (Figure 7). This isotopic distinction indicates that the amide phase observed in this study is distinct from

other N-bearing phases, potentially reflecting specific formation pathways under distinct environmental conditions.

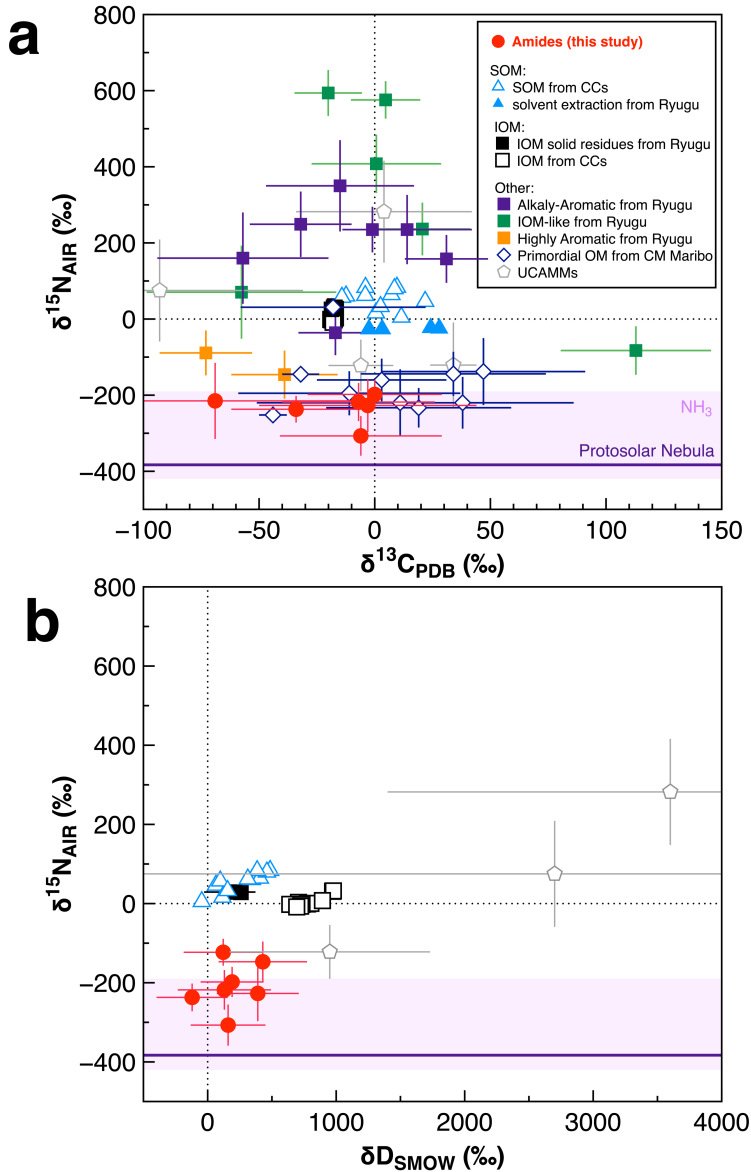


Figure 7. C, N and H isotopic compositions of the amides (red circles) detected in Ryugu's particle C0052 compared to literature data. (a) Plots of $\delta^{15}\text{N}$ vs. $\delta^{13}\text{C}$ and (b) $\delta^{15}\text{N}$ vs. δD for various classes of organic matter from Ryugu samples and carbonaceous chondrites, and ultra-carbonaceous Antarctic micrometeorites (UCAMMs, Rojas et al., 2024). The amides are compared to soluble organic matter (SOM), insoluble organic matter (IOM), and other C-rich organic grains from Ryugu (Takano et al., 2024; De Gregorio et al., 2024) and carbonaceous chondrites (Becker and Epstein, 1982; Alexander et al., 2007; Vollmer et al., 2020b). Black dashed lines correspond to terrestrial references, the solid purple line correspond to the $\delta^{15}\text{N}$ value of the protosolar nebula (Marty et al., 2011), and the colored pink region indicate the range of $\delta^{15}\text{N}$ values of NH_3 in cold molecular clouds (Gerin et al., 2009; Lis et al., 2010) . Uncertainties are 2σ .

4.3.2 Irradiation of ^{15}N depleted N-bearing ice?

Comparable depletions in ^{15}N as those found in Ryugu’s amides have been observed in “coldspots” within OM-like C-rich grains or nanoglobules in Ryugu samples (Nguyen et al., 2023; Yabuta et al., 2023; Stroud et al., 2024; De Gregorio et al., 2024), CM Maribo (Vollmer et al., 2020b), CO DOM 08006 (Nittler et al., 2018), CR chondrites (Floss and Stadermann, 2009; Floss et al., 2014; Vollmer et al., 2020a), and ultra-carbonaceous Antarctic micrometeorites (UCAMMs; Rojas et al., 2024) (Figure 7a). However, few studies have examined both the chemical and isotopic properties of these ^{15}N -depleted organic compounds in details. De Gregorio et al. (2024) reported two Ryugu grains in A0108-3, both depleted in ^{15}N and ^{13}C , with highly aromatic functional groups. In CM Maribo, Vollmer et al., (2020b) reported primordial ^{15}N -depleted organic material ($\delta^{15}\text{N} = -252\text{‰}$ to 31‰ , Figure 7a) dominated by aromatic and ketone/carbonyl ($\text{C}=\text{O}$) bonds, as well as $\text{C}=\text{N}/\text{C}\equiv\text{N}$ bonds. They suggested that this material may share an isotopic composition with HCN molecules from the ISM. In addition, Rojas et al., (2024) identified extremely light N bulk isotopic signatures in two UCAMMs rich in uncharacterized OM ($\delta^{15}\text{N} \simeq -120\text{‰}$, Figure 7a), proposing that these grains provide evidence of GCR irradiation of primordial ^{15}N -depleted N_2 ice on surface of cold objects from the outer regions of the Solar System.

The ^{15}N -depleted signature of the amides in our Ryugu samples is consistent with their formation from a ^{15}N -depleted reservoir. Amide-related components (e.g., formamide) can form through the irradiation of N-bearing ices (N_2 and NH_3) exposed to UV photons, energetic electrons or ions at low temperatures (<50 K) (Briggs et al., 1992; Gerakines et al., 2004; Jones et al., 2011; Kaňuchová et al., 2016). The protosolar nebula ($\delta^{15}\text{N} = -383 \pm 8\text{‰}$, Marty et al., 2011) and NH_3 in cold molecular clouds ($\delta^{15}\text{N}$ between -420‰ and -190‰ , (Gerin et al., 2009; Lis et al., 2010) exhibit lower or similar $\delta^{15}\text{N}$ compared to the N-H organic compounds in Ryugu. The isotopic fractionation of N during the formation of organic materials through ice irradiation remains poorly understood (Almayrac et al., 2022). However, experiments with UV and heavy ions irradiations of NH-bearing ice indicate little to no ^{15}N and D enrichment in the synthesized OM compared to the initial ices (Augé et al., 2019; Sugahara et al., 2019).

Therefore, a plausible scenario for the formation of ^{15}N -depleted amides in our Ryugu samples could involve the UV or GCR irradiations of ^{15}N -depleted N_2 or NH_3 -bearing ices either (*i*) at the surface of the Ryugu’s parent planetesimal in the outer Solar System, or (*ii*) on mantle of interstellar dust grains in the ISM before their accretion on the planetesimal. The former is consistent with other evidence indicating that Ryugu’s parent asteroid (and CI chondrites) likely formed beyond the H_2O and CO_2 snow lines (i.e., $\geq 3-15$ AU, (Desch et al., 2018; E. Nakamura et al., 2022; Hopp et al., 2022; Ito et al., 2022; Piani et al., 2023; Brunetto et al., 2023; Matsumoto et al., 2024; Maurel et al., 2024). However, the penetration of UV photons into chondritic material is weak (~ 100 nm), making their contribution highly unlikely. The penetration of

solar ions and GCR have a larger range, from nm to \sim 1 m. Over 4.55 billion of years, the accumulated dose can be as large as 10 eV/C atom. This raises the question about the exposure time of the Ryugu material at the surface of the parent body. Given that Ryugu formed from the recent collision of a large asteroid (Potiszil et al., 2023), it is clear that the exposure time ranges from zero to a few eV/C atoms. Consequently, no firm conclusion can be drawn. The exposure time at the surface of grains in the local ISM, or possibly in the outer regions of the protosolar disk, is around a few million years. Experimental simulations show that the effect of UV photons and swift heavy ions on CH₃OH:NH₃ mixtures are almost similar (Muñoz Caro et al., 2014). These experiments have identified amide functions in the molecular by-products, along with ions like OCN⁻ and NH₄⁺. Furthermore, irradiation-induced chemistry is observed at doses as low as 1 eV/C atom. Several studies also show that N₂ ice is radiolyzed under the effect of ion irradiation, leading to the formation of NH₃ and several N-rich molecular by-products (Palumbo et al., 2004; Augé et al., 2016; Rocha et al., 2020). It is therefore plausible that amide functions are formed by ion irradiation or UV photons in the ISM or the protosolar disk. However, due to the limited number of constraints, no definitive conclusion can be drawn.

5. Conclusions

In this study, we report the multi-scale (millimeter to nanometer) characterization of NH-bearing compounds in two Ryugu's particles (C0050 and C0052) from Chamber C. High-resolution AFM-IR imaging confirmed the presence of rare (\sim 1 vol.%), micrometer-sized amides (-C(=O)-NH-bearing organic compounds), unevenly distributed in Ryugu's particles. These amides are potential contributors, together with NH₄⁺ and amines, to the faint \sim 3.06 μ m absorption band observed at millimeter-scale on the global Ryugu grain collection (Pilorget et al., 2022). Combined AFM-IR and NanoSIMS analysis revealed that these amides have C and H isotopic compositions compatible with OM found in carbonaceous chondrites ($\delta^{13}\text{C} = -22 \pm 52\text{‰}$ and $\delta\text{D} = 194 \pm 368\text{‰}$), but they differ significantly in their N isotopic composition, being highly ¹⁵N-depleted ($\delta^{15}\text{N} = -215 \pm 92\text{‰}$). Although no amides have been recovered in Ryugu samples by chemical extraction so far, the ¹⁵N-depleted signature of the amides supports their indigenous origin in our samples.

The amides may have formed through aqueous alteration on the Ryugu's parent planetesimal or irradiation of ¹⁵N-depleted reservoir(s). Hydrothermal conditions could have led to amide formation from carboxylic acids and amine/NH₄⁺ precursors on the Ryugu's parent planetesimal, although isotopic analysis suggests that water-soluble organic molecules in Ryugu are enriched in ¹⁵N relative to the amides. Alternatively, the amides could have formed through irradiation of ¹⁵N-depleted ice (such as N₂ or NH₃) by UV photons or galactic cosmic rays in the outer Solar System or ISM.

C-type asteroids and comets may have delivered light elements and volatile organics to the inner Solar System, including early Earth (Chyba and Sagan, 1992; Martins and Pasek, 2024). Amides delivered on the early Earth by objects such as Ryugu, may have played a role in prebiotic chemistry.

Acknowledgments

The authors are very grateful to JAXA/ISAS Astromaterial Science Research Group for allowing the allocation of the two Ryugu's particles C0050 and C0052 to this research consortium through the first international Ryugu sample AO. We also acknowledge Frédéric Charlot for the assistance during SEM/EDS analysis at CMTC (Grenoble, France). This work has received support from H2020 European Research Council (ERC) (SOLARYS ERC-CoG2017_771691) and the Centre National d'Etudes Spatiales (CNES) within the framework of the Hayabusa2 and MMX missions. Lionel G. Vacher also acknowledges support from CNES, and Agence Nationale de la Recherche (ANR) CLASTS (ANR-22-CE49-0013) through post-doctoral grants.

Appendix

Data availability

The raw reflectance and μ -FTIR spectra are available online through the SSHADE Solid Spectroscopy database infrastructure with the following references: Beck and Poch (2022) for reflectance spectra and Vacher and Phan (2022) for μ -FTIR spectra.

References

- Alexander C. O., Fogel M., Yabuta H. and Cody G. D. (2007) The origin and evolution of chondrites recorded in the elemental and isotopic compositions of their macromolecular organic matter. *Geochim. Cosmochim. Acta* **71**, 4380–4403.
- Al-Kelani M. and Buthelezi N. (2024) Advancements in medical research: Exploring Fourier Transform Infrared (FTIR) spectroscopy for tissue, cell, and hair sample analysis. *Skin Res. Technol.* **30**, e13733.
- Almayrac M. G., Bekaert D. V., Broadley M. W., Byrne D. J., Piani L. and Marty B. (2022) The EXCITING Experiment Exploring the Behavior of Nitrogen and Noble Gases in Interstellar Ice Analogs. *Planet. Sci. J.* **3**, 252.
- Altwegg K., Balsiger H., Hänni N., Rubin M., Schuhmann M., Schroeder I., Sémon T., Wampfler S., Berthelier J.-J., Briois C., Combi M., Gombosi T. I., Cottin H., De Keyser J., Dhooghe F., Fiethé B. and Fuselier S. A. (2020) Evidence of ammonium salts in comet 67P as explanation for the nitrogen depletion in cometary comae. *Nat. Astron.* **4**, 533–540.
- Altwegg K., Combi M., Fuselier S. A., Hänni N., De Keyser J., Mahjoub A., Müller D. R., Pestoni B., Rubin M. and Wampfler S. F. (2022) Abundant ammonium hydrosulphide embedded in cometary dust grains. *Mon. Not. R. Astron. Soc.* **516**, 3900–3910.
- Amano K., Matsuoka M., Nakamura T., Kagawa E., Fujioka Y., Potin S. M., Hiroi T., Tatsumi E., Milliken R. E., Quirico E., Beck P., Brunetto R., Uesugi M., Takahashi Y., Kawai T., Yamashita S., Enokido Y., Wada T., Furukawa Y., Zolensky M. E., Takir D., Domingue D. L., Jaramillo-Correa C., Vilas F., Hendrix A. R., Kikuchi M., Morita T., Yurimoto H., Noguchi T., Okazaki R., Yabuta H., Naraoka H., Sakamoto K., Tachibana S., Yada T., Nishimura M., Nakato A., Miyazaki A., Yogata K., Abe M., Okada T., Usui T., Yoshikawa M., Saiki T., Tanaka S., Terui F., Nakazawa S., Watanabe S. and Tsuda Y. (2023) Reassigning CI chondrite parent bodies based on reflectance spectroscopy of samples from carbonaceous asteroid Ryugu and meteorites. *Sci. Adv.* **9**, eadi3789.
- Aponte J. C., Dworkin J. P. and Elsila J. E. (2014) Assessing the origins of aliphatic amines in the Murchison meteorite from their compound-specific carbon isotopic ratios and enantiomeric composition. *Geochim. Cosmochim. Acta* **141**, 331–345.
- Augé B., Dartois E., Duprat J., Engrand C., Slodzian G., Wu T. D., Guerquin-Kern J. L., Vermesse H., Agnihotri A. N., Boduch P. and Rothard H. (2019) Hydrogen isotopic anomalies in extraterrestrial organic matter: role of cosmic ray irradiation and implications for UCAMMs. *A&A* **627**.
- Augé B., Dartois E., Engrand C., Duprat J., Godard M., Delauche L., Bardin N., Mejía C., Martinez R., Muniz G., Domaracka A., Boduch P. and Rothard H. (2016) Irradiation of nitrogen-rich ices by swift heavy ions: Clues for the formation of ultracarbonaceous micrometeorites. *Astron. Astrophys.* **592**, A99.
- Beaumont V. and Robert F. (1999) Nitrogen isotope ratios of kerogens in Precambrian cherts: a record of the evolution of atmosphere chemistry? *Precambrian Res.* **96**, 63–82.
- Beck P., Quirico E., Montes-Hernandez G., Bonal L., Bolland J., Orthous-Daunay F.-R., Howard K. T., Schmitt B., Brissaud O. and Deschamps F. (2010) Hydrous mineralogy of CM and CI chondrites

from infrared spectroscopy and their relationship with low albedo asteroids. *Geochim. Cosmochim. Acta* **74**, 4881–4892.

Beck P and Poch O. (2022): Vis-NIR reflectance spectra ($i = 0^\circ$, $e = 20^\circ$) of Chamber C Ryugu individual raw particles C0050 and C0052 (Hayabusa2 mission, JAXA) placed in a cell under N2 atmosphere. SSHADE/GhoSST (OSUG Data Center). Dataset/Spectral Data. doi:[10.26302/SSHADE/EXPERIMENT_LB_20241122_001](https://doi.org/10.26302/SSHADE/EXPERIMENT_LB_20241122_001).

Becker R. H. and Epstein S. (1982) Carbon, hydrogen and nitrogen isotopes in solvent-extractable organic matter from carbonaceous chondrites. *Geochim. Cosmochim. Acta* **46**, 97–103.

Bonal L., Quirico E., Montagnac G., Komatsu M., Kebukawa Y., Yabuta H., Amano K., Barosch J., Bejach L., Cody G. D., Dartois E., Dazzi A., De Gregorio B., Deniset-Besseau A., Duprat J., Engrand C., Hashiguchi M., Kamide K., Kilcoyne D., Martins Z., Mathurin J., Mostefaoui S., Nittler L., Ohigashi T., Okumura T., Remusat L., Sandford S., Shigenaka M., Stroud R., Suga H., Takahashi Y., Takeichi Y., Tamenori Y., Verdier-Paoletti M., Yamashita S., Nakamura T., Naraoka H., Noguchi T., Okazaki R., Yurimoto H., Tachibana S., Abe M., Miyazaki A., Nakato A., Nakazawa S., Nishimura M., Okada T., Saiki T., Sakamoto K., Tanaka S., Terui F., Tsuda Y., Usui T., Watanabe S., Yada T., Yogata K. and Yoshikawa M. (2024) The thermal history of Ryugu based on Raman characterization of Hayabusa2 samples. *Icarus* **408**, 115826.

Briggs R., Ertem G., Ferris J. P., Greenberg J. M., McCain P. J., Mendoza-Gomez C. X. and Schutte W. (1992) Comet Halley as an aggregate of interstellar dust and further evidence for the photochemical formation of organics in the interstellar medium. *Orig. Life Evol. Biosph.* **22**, 287–307.

Brunetto R., Lantz C., Fukuda Y., Aléon-Toppani A., Nakamura T., Dionnet Z., Baklouti D., Borondics F., Djouadi Z., Rubino S., Amano K., Matsumoto M., Fujioka Y., Morita T., Kukui M., Kagawa E., Matsuoka M., Milliken R., Yurimoto H., Noguchi T., Okazaki R., Yabuta H., Naraoka H., Sakamoto K., Tachibana S., Yada T., Nishimura M., Nakato A., Miyazaki A., Yogata K., Abe M., Okada T., Usui T., Yoshikawa M., Saiki T., Tanaka S., Terui F., Nakazawa S., Watanabe S. and Tsuda Y. (2023) Ryugu's Anhydrous Ingredients and Their Spectral Link to Primitive Dust from the Outer Solar System. *Astrophys. J. Lett.* **951**, L33.

Burton A. S., Grunsfeld S., Elsila J. E., Glavin D. P. and Dworkin J. P. (2014) The effects of parent-body hydrothermal heating on amino acid abundances in CI-like chondrites. *Polar Sci.* **8**, 255–263.

Chyba C. and Sagan C. (1992) Endogenous production, exogenous delivery and impact-shock synthesis of organic molecules: an inventory for the origins of life. *Nature* **355**, 125–132.

Cooper G. W. and Cronin J. R. (1995) Linear and cyclic aliphatic carboxamides of the Murchison meteorite: Hydrolyzable derivatives of amino acids and other carboxylic acids. *Geochim. Cosmochim. Acta* **59**, 1003–1015.

Cronin J. R. (1976a) Acid-labile amino acid precursors in the Murchison meteorite: 1: Chromatographic fractionation. *Orig. Life* **7**, 337–342.

Cronin J. R. (1976b) Acid-labile amino acid precursors in the Murchison meteorite: II: A search for peptides and amino acyl amides. *Orig. Life* **7**, 343–348.

Dartois E., Kebukawa Y., Yabuta H., Mathurin J., Engrand C., Duprat J., Bejach L., Dazzi A., Deniset-Besseau A., Bonal L., Quirico E., Sandt C., Borondics F., Barosch J., Cody G. D., De Gregorio B.

T., Hashiguchi M., Kilcoyne D. A. L., Komatsu M., Martins Z., Matsumoto M., Montagnac G., Mostefaoui S., Nittler L. R., Ohigashi T., Okumura T., Remusat L., Sandford S., Shigenaka M., Stroud R., Suga H., Takahashi Y., Takeichi Y., Tamenori Y., Verdier-Paoletti M., Yamashita S., Nakamura T., Morita T., Kikuiri M., Amano K., Kagawa E., Noguchi T., Naraoka H., Okazaki R., Sakamoto K., Yurimoto H., Abe M., Kamide K., Miyazaki A., Nakato A., Nakazawa S., Nishimura M., Okada T., Saiki T., Tachibana S., Tanaka S., Terui F., Tsuda Y., Usui T., Watanabe S., Yada T., Yogata K. and Yoshikawa M. (2023) Chemical composition of carbonaceous asteroid Ryugu from synchrotron spectroscopy in the mid- to far-infrared of Hayabusa2-returned samples. *A&A* **671**.

De Gregorio B., Cody G. D., Stroud R. M., David Kilcoyne A. L., Sandford S., Le Guillou C., Nittler L. R., Barosch J., Yabuta H., Martins Z., Kebukawa Y., Okumura T., Hashiguchi M., Yamashita S., Takeichi Y., Takahashi Y., Wakabayashi D., Engrand C., Bejach L., Bonal L., Quirico E., Remusat L., Duprat J., Verdier-Paoletti M., Mostefaoui S., Komatsu M., Mathurin J., Dazzi A., Deniset-Besseau A., Dartois E., Tamenori Y., Suga H., Montagnac G., Kamide K., Shigenaka M., Matsumoto M., Enokido Y., Yoshikawa M., Saiki T., Tanaka S., Terui F., Nakazawa S., Usui T., Abe M., Okada T., Yada T., Nishimura M., Nakato A., Miyazaki A., Yogata K., Yurimoto H., Nakamura T., Noguchi T., Okazaki R., Naraoka H., Sakamoto K., Tachibana S., Watanabe S. and Tsuda Y. (2024) Variations of organic functional chemistry in carbonaceous matter from the asteroid 162173 Ryugu. *Nat. Commun.* **15**, 7488.

De Sanctis M. C., Ammannito E., Raponi A., Marchi S., McCord T. B., McSween H. Y., Capaccioni F., Capria M. T., Carrozzo F. G., Ciarniello M., Longobardo A., Tosi F., Fonte S., Formisano M., Frigeri A., Giardino M., Magni G., Palomba E., Turrini D., Zambon F., Combe J.-P., Feldman W., Jaumann R., McFadden L. A., Pieters C. M., Prettyman T., Toplis M., Raymond C. A. and Russell C. T. (2015) Ammoniated phyllosilicates with a likely outer Solar System origin on (1) Ceres. *Nature* **528**, 241–244.

Desch S. J., Kalyaan A. and Alexander C. M. (2018) The effect of Jupiter's formation on the distribution of refractory elements and inclusions in meteorites. *Astrophys. J. Suppl. Ser.* **238**, 11.

Elsila J. E., Callahan M. P., Dworkin J. P., Glavin D. P., McLain H. L., Noble S. K. and Gibson E. K. (2016) The origin of amino acids in lunar regolith samples. *Geochim. Cosmochim. Acta* **172**, 357–369.

Fastelli M., Comodi P., Maturilli A. and Zucchini A. (2020) Reflectance Spectroscopy of Ammonium Salts: Implications for Planetary Surface Composition. *Minerals* **10**.

Floss C., Le Guillou C. and Brarley A. (2014) Coordinated NanoSIMS and FIB-TEM analyses of organic matter and associated matrix materials in CR3 chondrites. *Geochim. Cosmochim. Acta* **139**, 1–25.

Floss C. and Stadermann F. J. (2009) HIGH ABUNDANCES OF CIRCUMSTELLAR AND INTERSTELLAR C-ANOMALOUS PHASES IN THE PRIMITIVE CR3 CHONDRITES QUE 99177 AND MET 00426. *Astrophys. J.* **697**, 1242.

Fu X., Liao Y., Glein C. R., Jamison M., Hayes K., Zaporski J. and Yang Z. (2020) Direct Synthesis of Amides from Amines and Carboxylic Acids under Hydrothermal Conditions. *ACS Earth Space Chem.* **4**, 722–729.

Für E. and Marty B. (2015) Nitrogen isotope variations in the Solar System. *Nat. Geosci.* **8**, 515–522.

Gerakines P. A., Moore M. H. and Hudson R. L. (2004) Ultraviolet photolysis and proton irradiation of astrophysical ice analogs containing hydrogen cyanide. *Icarus* **170**, 202–213.

Gerin M., Marcelino N., Biver N., Roueff E., Coudert L. H., Elkeurti M., Lis D. C. and Bockelée-Morvan D. (2009) Detection of $^{15}\text{NH}_2\text{D}$ in dense cores: a new tool for measuring the $^{14}\text{N}/^{15}\text{N}$ ratio in the cold ISM*. *A&A* **498**, L9–L12.

Glavin D. P., McLain H. L., Dworkin J. P., Parker E. T., Elsila J. E., Aponte J. C., Simkus D. N., Pozarycki C. I., Graham H. V., Nittler L. R. and Alexander C. M. O. (2020) Abundant extraterrestrial amino acids in the primitive CM carbonaceous chondrite Asuka 12236. *Meteorit. Planet. Sci.* **55**, 1979–2006.

Grewal D. S. (2022) Origin of Nitrogen Isotopic Variations in the Rocky Bodies of the Solar System. *Astrophys. J.* **937**, 123.

Hatakeyama K., Yada T., Abe M., Okada T., Nakato A., Yogata K., Miyazaki A., Kumagai K., Nishimura M., Hitomi Y., Soejima H., Nagashima K., Yoshitake M., Iwamae A., Furuya S., Usui T. and Kitazato K. (2023) Homogeneity and heterogeneity in near-infrared FTIR spectra of Ryugu returned samples. *Earth Planets Space* **75**, 46.

Hily-Blant P., Magalhaes de Souza V., Kastner J. and Forveille T. (2019) Multiple nitrogen reservoirs in a protoplanetary disk at the epoch of comet and giant planet formation. *A&A* **632**.

Hopp T., Dauphas N., Abe Y., Aléon J., O'D. Alexander C. M., Amari S., Amelin Y., Bajo K., Bizzarro M., Bouvier A., Carlson R. W., Chaussidon M., Choi B.-G., Davis A. M., Di Rocco T., Fujiya W., Fukai R., Gautam I., Haba M. K., Hibiya Y., Hidaka H., Homma H., Hoppe P., Huss G. R., Ichida K., Iizuka T., Ireland T. R., Ishikawa A., Ito M., Itoh S., Kawasaki N., Kita N. T., Kitajima K., Kleine T., Komatani S., Krot A. N., Liu M.-C., Masuda Y., McKeegan K. D., Morita M., Motomura K., Moynier F., Nakai I., Nagashima K., Nesvorný D., Nguyen A., Nittler L., Onose M., Pack A., Park C., Piani L., Qin L., Russell S. S., Sakamoto N., Schönbächler M., Tafla L., Tang H., Terada K., Terada Y., Usui T., Wada S., Wadhwa M., Walker R. J., Yamashita K., Yin Q.-Z., Yokoyama T., Yoneda S., Young E. D., Yui H., Zhang A.-C., Nakamura T., Naraoka H., Noguchi T., Okazaki R., Sakamoto K., Yabuta H., Abe M., Miyazaki A., Nakato A., Nishimura M., Okada T., Yada T., Yogata K., Nakazawa S., Saiki T., Tanaka S., Terui F., Tsuda Y., Watanabe S., Yoshikawa M., Tachibana S. and Yurimoto H. (2022) Ryugu's nucleosynthetic heritage from the outskirts of the Solar System. *Sci. Adv.* **8**, eadd8141.

Ito M., Takano Y., Kebukawa Y., Ohigashi T., Matsuoka M., Kiryu K., Uesugi M., Nakamura T., Yuzawa H., Yamada K., Naraoka H., Yada T., Abe M., Hayakawa M., Saiki T., Tachibana S., and Hayabusa II Project Team (2021) Assessing the debris generated by the small carry-on impactor operated from the Hayabusa2 mission. *Geochim. J.* **55**, 223–239.

Ito M., Tomioka N., Uesugi M., Yamaguchi A., Shirai N., Ohigashi T., Liu M.-C., Greenwood R. C., Kimura M., Imae N., Uesugi K., Nakato A., Yogata K., Yuzawa H., Kodama Y., Tsuchiyama A., Yasutake M., Findlay R., Franchi I. A., Malley J. A., McCain K. A., Matsuda N., McKeegan K. D., Hirahara K., Takeuchi A., Sekimoto S., Sakurai I., Okada I., Karouji Y., Arakawa M., Fujii A., Fujimoto M., Hayakawa M., Hirata Naoyuki, Hirata Naru, Honda R., Honda C., Hosoda S., Iijima Y., Ikeda H., Ishiguro M., Ishihara Y., Iwata T., Kawahara K., Kikuchi S., Kitazato K., Matsumoto K., Matsuoka M., Michikami T., Mimasu Y., Miura A., Mori O., Morota T., Nakazawa S., Namiki N., Noda H., Noguchi R., Ogawa N., Ogawa K., Okada T., Okamoto C., Ono G., Ozaki M., Saiki T., Sakatani N., Sawada H., Senshu H., Shimaki Y., Shirai K., Sugita S., Takei Y., Takeuchi H.,

Tanaka S., Tatsumi E., Terui F., Tsukizaki R., Wada K., Yamada M., Yamada T., Yamamoto Y., Yano H., Yokota Y., Yoshihara K., Yoshikawa M., Yoshikawa K., Fukai R., Furuya S., Hatakeda K., Hayashi T., Hitomi Y., Kumagai K., Miyazaki A., Nishimura M., Soejima H., Iwamae A., Yamamoto D., Yoshitake M., Yada T., Abe M., Usui T., Watanabe S. and Tsuda Y. (2022) A pristine record of outer Solar System materials from asteroid Ryugu's returned sample. *Nat. Astron.* **6**, 1163–1171.

Ji Y., Yang X., Ji Z., Zhu L., Ma N., Chen D., Jia X., Tang J. and Cao Y. (2020) DFT-Calculated IR Spectrum Amide I, II, and III Band Contributions of N-Methylacetamide Fine Components. *ACS Omega* **5**, 8572–8578.

Jiang T., Pilorget C., Loizeau D., Bibring J.-P., Yogata K., Hatakeda K., Brunetto R., Le Pivert-Jolivert T., Lantz C. and Riu L. (2024) NH-Rich Grains Detected by MicrOmega in the Ryugu Returned Samples. *LPI Contrib.* **3040**, 1522.

Jones B. M., Bennett C. J. and Kaiser R. I. (2011) MECHANISTICAL STUDIES ON THE PRODUCTION OF FORMAMIDE (H₂NCHO) WITHIN INTERSTELLAR ICE ANALOGS. *Astrophys. J.* **734**, 78.

Kaňuchová Z., Urso R. G., Baratta G. A., Brucato J. R., Palumbo M. E. and Strazzulla G. (2016) Synthesis of formamide and isocyanic acid after ion irradiation of frozen gas mixtures. *A&A* **585**.

Kebukawa Y., Alexander C. M. O. and Cody G. D. (2019a) Comparison of FT-IR spectra of bulk and acid insoluble organic matter in chondritic meteorites: An implication for missing carbon during demineralization. *Meteorit. Planet. Sci.* **54**, 1632–1641.

Kebukawa Y., Alexander C. M. O. and Cody G. D. (2011) Compositional diversity in insoluble organic matter in type 1, 2 and 3 chondrites as detected by infrared spectroscopy. *Geochim. Cosmochim. Acta* **75**, 3530–3541.

Kebukawa Y., Kobayashi H., Urayama N., Baden N., Kondo M., Zolensky M. E. and Kobayashi K. (2019b) Nanoscale infrared imaging analysis of carbonaceous chondrites to understand organic-mineral interactions during aqueous alteration. *Proc. Natl. Acad. Sci.* **116**, 753–758.

Kebukawa Y., Mathurin J., Dartois E., Dazzi A., Deniset-Besseau A., Duprat J., Remusat L., Noguchi T., Miyake A., Igami Y., Paoletti M. V., Zolensky M. E., Engrand C., Sandt C., Borondics F., Yamashita S., Wakabayashi D., Takeichi Y. and Takahashi Y. (2023) Complex mixture of organic matter in a xenolithic clast from the Zag meteorite revealed by coordinated analyses using AFM-IR, NanoSIMS and STXM/XANES. *Icarus* **400**, 115582.

Kebukawa Y., Quirico E., Dartois E., Yabuta H., Bejach L., Bonal L., Dazzi A., Deniset-Besseau A., Duprat J., Engrand C., Mathurin J., Barosch J., Cody G. D., De Gregorio B., Hashiguchi M., Kamide K., Kilcoyne D., Komatsu M., Martins Z., Montagnac G., Mostefaoui S., Nittler L. R., Ohigashi T., Okumura T., Remusat L., Sandford S., Shigenaka M., Stroud R., Suga H., Takahashi Y., Takeichi Y., Tamenori Y., Verdier-Paoletti M., Wakabayashi D., Yamashita S., Yurimoto H., Nakamura T., Noguchi T., Okazaki R., Naraoka H., Sakamoto K., Tachibana S., Yada T., Nishimura M., Nakato A., Miyazaki A., Yogata K., Abe M., Okada T., Usui T., Yoshikawa M., Saiki T., Tanaka S., Terui F., Nakazawa S., Watanabe S. and Tsuda Y. (2024) Infrared absorption spectra from organic matter in the asteroid Ryugu samples: Some unique properties compared to unheated carbonaceous chondrites. *Meteorit. Planet. Sci.* **59**, 1845–1858.

- King T. V. V., Clark R. N., Calvin W. M., Sherman D. M. and Brown R. H. (1992) Evidence for Ammonium-Bearing Minerals on Ceres. *Science* **255**, 1551–1553.
- Lange J., Djago F., Eddhif B., Remaury Q. B., Ruf A., Leitner N. K. V., d'Hendecourt L. L. S., Danger G., Rodier C. G., Papot S. and Poinot P. (2020) Evidence for Proteogenic Peptide-like Sequences in Meteorites Through an Enzyme-Catalysed Stereoselective Hydrolysis Strategy.
- Lin-Vien D., Colthup N. B., Fateley W. G. and Grasselli J. G. (1991) *The handbook of infrared and Raman characteristic frequencies of organic molecules.*, Elsevier.
- Lis D. C., Wootten A., Gerin M. and Roueff E. (2010) Nitrogen Isotopic Fractionation in Interstellar Ammonia. *Astrophys. J. Lett.* **710**, L49.
- Marlier J. F., Dopke N. C., Johnstone K. R. and Wirdzic T. J. (1999) A Heavy-Atom Isotope Effect Study of the Hydrolysis of Formamide. *J. Am. Chem. Soc.* **121**, 4356–4363.
- Martins Z. and Pasek M. A. (2024) Delivery of Organic Matter to the Early Earth. *Elements* **20**, 19–23.
- Marty B., Chaussidon M., Wiens R. C., Jurewicz A. J. G. and Burnett D. S. (2011) A ^{15}N -Poor Isotopic Composition for the Solar System As Shown by Genesis Solar Wind Samples. *Science* **332**, 1533–1536.
- Mathurin J., Dartois E., Pino T., Engrand C., Duprat J., Deniset-besseau A., Borondics F., Sandt C. and Dazzi A. (2019) Nanometre-scale infrared chemical imaging of organic matter in ultra-carbonaceous Antarctic micrometeorites (UCAMMs). *Astron. Astrophys.* **160**, 1–9.
- Matsumoto T., Noguchi T., Miyake A., Igami Y., Haruta M., Seto Y., Miyahara M., Tomioka N., Saito H., Hata S., Harries D., Takigawa A., Nakauchi Y., Tachibana S., Nakamura T., Matsumoto M., Ishii H. A., Bradley J. P., Ohtaki K., Dobrică E., Leroux H., Le Guillou C., Jacob D., de la Peña F., Laforet S., Marinova M., Langenhorst F., Beck P., Phan T. H. V., Rebois R., Abreu N. M., Gray J., Zega T., Zanetta P.-M., Thompson M. S., Stroud R., Burgess K., Cymes B. A., Bridges J. C., Hicks L., Lee M. R., Daly L., Bland P. A., Zolensky M. E., Frank D. R., Martinez J., Tsuchiyama A., Yasutake M., Matsuno J., Okumura S., Mitsukawa I., Uesugi K., Uesugi M., Takeuchi A., Sun M., Enju S., Michikami T., Yurimoto H., Okazaki R., Yabuta H., Naraoka H., Sakamoto K., Yada T., Nishimura M., Nakato A., Miyazaki A., Yogata K., Abe M., Okada T., Usui T., Yoshikawa M., Saiki T., Tanaka S., Terui F., Nakazawa S., Watanabe S. and Tsuda Y. (2024) Influx of nitrogen-rich material from the outer Solar System indicated by iron nitride in Ryugu samples. *Nat. Astron.* **8**, 207–215.
- Maurel C., Gattacceca J. and Uehara M. (2024) Hayabusa 2 returned samples reveal a weak to null magnetic field during aqueous alteration of Ryugu's parent body. *Earth Planet. Sci. Lett.* **627**, 118559.
- McGeoch J. E. M. and McGeoch M. W. (2015) Polymer amide in the Allende and Murchison meteorites. *Meteorit. Planet. Sci.* **50**, 1971–1983.
- Meierhenrich U. J., Muñoz Caro G. M., Bredehöft J. H., Jessberger E. K. and Thiemann W. H.-P. (2004) Identification of diamino acids in the Murchison meteorite. *Proc. Natl. Acad. Sci.* **101**, 9182–9186.
- Muñoz Caro G. M., Dartois E., Boduch P., Rothard H., Domaracka A. and Jiménez-Escobar A. (2014) Comparison of UV and high-energy ion irradiation of methanol:ammonia ice. *A&A* **566**.

Nakamura E., KOBAYASHI K., TANAKA R., KUNIHIRO T., KITAGAWA H., POTISZIL C., OTA T., SAKAGUCHI C., YAMANAKA M., RATNAYAKE D. M., TRIPATHI H., KUMAR R., AVRAMESCU M.-L., TSUCHIDA H., YACHI Y., MIURA H., ABE M., FUKAI R., FURUYA S., HATAKEDA K., HAYASHI T., HITOMI Y., KUMAGAI K., MIYAZAKI A., NAKATO A., NISHIMURA M., OKADA T., SOEJIMA H., SUGITA S., SUZUKI A., USUI T., YADA T., YAMAMOTO D., YOGATA K., YOSHITAKE M., ARAKAWA M., FUJII A., HAYAKAWA M., HIRATA Naoyuki, HIRATA Naru, HONDA R., HONDA C., HOSODA S., IIJIMA Y., IKEDA H., ISHIGURO M., ISHIHARA Y., IWATA T., KAWAHARA K., KIKUCHI S., KITAZATO K., MATSUMOTO K., MATSUOKA M., MICHIKAMI T., MIMASU Y., MIURA A., MOROTA T., NAKAZAWA S., NAMIKI N., NODA H., NOGUCHI R., OGAWA N., OGAWA K., OKAMOTO C., ONO G., OZAKI M., SAIKI T., SAKATANI N., SAWADA H., SENSHU H., SHIMAKI Y., SHIRAI K., TAKEI Y., TAKEUCHI H., TANAKA S., TATSUMI E., TERUI F., TSUKIZAKI R., WADA K., YAMADA M., YAMADA T., YAMAMOTO Y., YANO H., YOKOTA Y., YOSHIHARA K., YOSHIKAWA M., YOSHIKAWA K., FUJIMOTO M., WATANABE S. and TSUDA Y. (2022) On the origin and evolution of the asteroid Ryugu: A comprehensive geochemical perspective. *Proc. Jpn. Acad. Ser. B* **98**, 227–282.

Nakamura T., Matsumoto M., Amano K., Enokido Y., Zolensky M. E., Mikouchi T., Genda H., Tanaka S., Zolotov M. Y., Kurosawa K., Wakita S., Hyodo R., Nagano H., Nakashima D., Takahashi Y., Fujioka Y., Kikui M., Kagawa E., Matsuoka M., Brearley A. J., Tsuchiyama A., Uesugi M., Matsuno J., Kimura Y., Sato M., Milliken R. E., Tatsumi E., Sugita S., Hiroi T., Kitazato K., Brownlee D., Joswiak D. J., Takahashi M., Ninomiya K., Takahashi T., Osawa T., Terada K., Brenker F. E., Tkalcic B. J., Vincze L., Brunetto R., Aléon-Toppani A., Chan Q. H. S., Roskosz M., Viennet J.-C., Beck P., Alp E. E., Michikami T., Nagaashi Y., Tsuji T., Ino Y., Martinez J., Han J., Dolocan A., Bodnar R. J., Tanaka M., Yoshida H., Sugiyama K., King A. J., Fukushi K., Suga H., Yamashita S., Kawai T., Inoue K., Nakato A., Noguchi T., Vilas F., Hendrix A. R., Jaramillo-Correa C., Domingue D. L., Dominguez G., Gainsforth Z., Engrand C., Duprat J., Russell S. S., Bonato E., Ma C., Kawamoto T., Wada T., Watanabe S., Endo R., Enju S., Riu L., Rubino S., Tack P., Takeshita S., Takeichi Y., Takeuchi A., Takigawa A., Takir D., Tanigaki T., Taniguchi A., Tsukamoto K., Yagi T., Yamada S., Yamamoto K., Yamashita Y., Yasutake M., Uesugi K., Umegaki I., Chiu I., Ishizaki T., Okumura S., Palomba E., Pilorget C., Potin S. M., Alasli A., Anada S., Araki Y., Sakatani N., Schultz C., Sekizawa O., Sitzman S. D., Sugiura K., Sun M., Dartois E., De Pauw E., Dionnet Z., Djouadi Z., Falkenberg G., Fujita R., Fukuma T., Gearba I. R., Hagiya K., Hu M. Y., Kato T., Kawamura T., Kimura M., Kubo M. K., Langenhorst F., Lantz C., Lavina B., Lindner M., Zhao J., Vekemans B., Baklouti D., Bazi B., Borondics F., Nagasawa S., Nishiyama G., Nitta K., Mathurin J., Matsumoto T., Mitsukawa I., Miura H., Miyake A., Miyake Y., Yurimoto H., Okazaki R., Yabuta H., Naraoka H., Sakamoto K., Tachibana S., Connolly H. C., Lauretta D. S., Yoshitake M., Yoshikawa M., Yoshikawa K., Yoshihara K., Yokota Y., Yogata K., Yano H., Yamamoto Y., Yamamoto D., Yamada M., Yamada T., Yada T., Wada K., Usui T., Tsukizaki R., Terui F., Takeuchi H., Takei Y., Iwamae A., Soejima H., Shirai K., Shimaki Y., Senshu H., Sawada H., Saiki T., Ozaki M., Ono G., Okada T., Ogawa N., Ogawa K., Noguchi R., Noda H., Nishimura M., Namiki N., Nakazawa S., Morota T., Miyazaki A., Miura A., Mimasu Y., Matsumoto K., Kumagai K., Kouyama T., Kikuchi S., Kawahara K., Kameda S., Iwata T., Ishihara Y., Ishiguro M., Ikeda H., Hosoda S., Honda R., Honda C., Hitomi Y., Hirata N., Hirata N., Hayashi T., Hayakawa M., Hatakeda K., Furuya S., Fukai R., Fujii A., Cho Y., Arakawa M., Abe M., Watanabe S. and Tsuda Y. (2022) Formation and evolution of carbonaceous asteroid Ryugu: Direct evidence from returned samples. *Science* **379**, eabn8671.

Naraoka H., Takano Y., Dworkin J. P., Oba Y., Hamase K., Furusho A., Ogawa N. O., Hashiguchi M., Fukushima K., Aoki D., Schmitt-Kopplin P., Aponte J. C., Parker E. T., Glavin D. P., McLain H. L., Elsila J. E., Graham H. V., Eiler J. M., Orthous-Daunay F.-R., Wolters C., Isa J., Vuitton V.,

Thissen R., Sakai S., Yoshimura T., Koga T., Ohkouchi N., Chikaraishi Y., Sugahara H., Mita H., Furukawa Y., Hertkorn N., Ruf A., Yurimoto H., Nakamura T., Noguchi T., Okazaki R., Yabuta H., Sakamoto K., Tachibana S., Connolly H. C., Lauretta D. S., Abe M., Yada T., Nishimura M., Yogata K., Nakato A., Yoshitake M., Suzuki A., Miyazaki A., Furuya S., Hatakeyama K., Soejima H., Hitomi Y., Kumagai K., Usui T., Hayashi T., Yamamoto D., Fukai R., Kitazato K., Sugita S., Namiki N., Arakawa M., Ikeda H., Ishiguro M., Hirata Naru, Wada K., Ishihara Y., Noguchi R., Morota T., Sakatani N., Matsumoto K., Senshu H., Honda R., Tatsumi E., Yokota Y., Honda C., Michikami T., Matsuoka M., Miura A., Noda H., Yamada T., Yoshihara K., Kawahara K., Ozaki M., Iijima Y., Yano H., Hayakawa M., Iwata T., Tsukizaki R., Sawada H., Hosoda S., Ogawa K., Okamoto C., Hirata Naoyuki, Shirai K., Shimaki Y., Yamada M., Okada T., Yamamoto Y., Takeuchi H., Fujii A., Takei Y., Yoshikawa K., Mimasu Y., Ono G., Ogawa N., Kikuchi S., Nakazawa S., Terui F., Tanaka S., Saiki T., Yoshikawa M., Watanabe S. and Tsuda Y. (2023) Soluble organic molecules in samples of the carbonaceous asteroid (162173) Ryugu. *Science* **379**, eabn9033.

Nguyen A. N., Mane P., Keller L. P., Piani L., Abe Y., Aléon J., Alexander C. M. O., Amari S., Amelin Y., Bajo K., Bizzarro M., Bouvier A., Carlson R. W., Chaussidon M., Choi B.-G., Dauphas N., Davis A. M., Di Rocco T., Fujiya W., Fukai R., Gautam I., Haba M. K., Hibiya Y., Hidaka H., Homma H., Hoppe P., Huss G. R., Ichida K., Iizuka T., Ireland T. R., Ishikawa A., Itoh S., Kawasaki N., Kita N. T., Kitajima K., Kleine T., Komatani S., Krot A. N., Liu M.-C., Masuda Y., McKeegan K. D., Morita M., Motomura K., Moynier F., Nakai I., Nagashima K., Nesvorný D., Nittler L., Onose M., Pack A., Park C., Qin L., Russell S. S., Sakamoto N., Schönbächler M., Tafla L., Tang H., Terada K., Terada Y., Usui T., Wada S., Wadhwa M., Walker R. J., Yamashita K., Yin Q.-Z., Yokoyama T., Yoneda S., Young E. D., Yui H., Zhang A.-C., Nakamura T., Naraoka H., Noguchi T., Okazaki R., Sakamoto K., Yabuta H., Abe M., Miyazaki A., Nakato A., Nishimura M., Okada T., Yada T., Yogata K., Nakazawa S., Saiki T., Tanaka S., Terui F., Tsuda Y., Watanabe S., Yoshikawa M., Tachibana S. and Yurimoto H. (2023) Abundant presolar grains and primordial organics preserved in carbon-rich exogenous clasts in asteroid Ryugu. *Sci. Adv.* **9**, eadh1003.

Nittler L. R., Alexander C. M. O., Davidson J., Riebe M. E. I., Stroud R. M. and Wang J. (2018) High abundances of presolar grains and 15N-rich organic matter in CO3.0 chondrite Dominion Range 08006. *Geochim. Cosmochim. Acta* **226**, 107–131.

Oba Y., Koga T., Takano Y., Ogawa N. O., Ohkouchi N., Sasaki K., Sato H., Glavin D. P., Dworkin J. P., Naraoka H., Tachibana S., Yurimoto H., Nakamura T., Noguchi T., Okazaki R., Yabuta H., Sakamoto K., Yada T., Nishimura M., Nakato A., Miyazaki A., Yogata K., Abe M., Okada T., Usui T., Yoshikawa M., Saiki T., Tanaka S., Terui F., Nakazawa S., Watanabe S., Tsuda Y., and Hayabusa2-initial-analysis SOM team (2023) Uracil in the carbonaceous asteroid (162173) Ryugu. *Nat. Commun.* **14**, 1292.

Ogliore R., Nagashima K., Huss G. and Haenecour P. (2021) A reassessment of the quasi-simultaneous arrival effect in secondary ion mass spectrometry. *Nucl. Instrum. Methods Phys. Res. Sect. B Beam Interact. Mater. At.* **491**, 17–28.

Orthous-Daunay F.-R., Quirico E., Beck P., Brissaud O., Dartois E., Pino T. and Schmitt B. (2013) Mid-infrared study of the molecular structure variability of insoluble organic matter from primitive chondrites. *Icarus* **223**, 534–543.

Orthous-Daunay F.-R., Quirico E., Lemelle L., Beck P., deAndrade V., Simionovici A. and Derenne S. (2010) Speciation of sulfur in the insoluble organic matter from carbonaceous chondrites by XANES spectroscopy. *Earth Planet. Sci. Lett.* **300**, 321–328.

Palme H., Lodders K. and Jones A. (2014) 2.2 - Solar System Abundances of the Elements A2 - Holland, Heinrich D. In *Treatise on Geochemistry (Second Edition)* (ed. K. K. Turekian). Elsevier, Oxford. pp. 15–36.

Palumbo M. E., Ferini G. and Baratta G. A. (2004) Infrared and Raman spectroscopies of refractory residues left over after ion irradiation of nitrogen-bearing icy mixtures. *Adv. Space Res.* **33**, 49–56.

Parker E. T., McLain H. L., Glavin D. P., Dworkin J. P., Elsila J. E., Aponte J. C., Naraoka H., Takano Y., Tachibana S., Yabuta H., Yurimoto H., Sakamoto K., Yada T., Nishimura M., Nakato A., Miyazaki A., Yogata K., Abe M., Okada T., Usui T., Yoshikawa M., Saiki T., Tanaka S., Nakazawa S., Tsuda Y., Terui F., Noguchi T., Okazaki R., Watanabe S. and Nakamura T. (2023) Extraterrestrial amino acids and amines identified in asteroid Ryugu samples returned by the Hayabusa2 mission. *Geochim. Cosmochim. Acta* **347**, 42–57.

Petit S., Righi D. and Madejová J. (2006) Infrared spectroscopy of NH₄⁺-bearing and saturated clay minerals: A review of the study of layer charge. *Layer Charge Clay Miner.* **34**, 22–30.

Petzke K. J., Boeing H., Klaus S. and Metges C. C. (2005) Carbon and Nitrogen Stable Isotopic Composition of Hair Protein and Amino Acids Can Be Used as Biomarkers for Animal-Derived Dietary Protein Intake in Humans. *J. Nutr.* **135**, 1515–1520.

Phan V. T. H., Beck P., Rebois R., Quirico E., Noguchi T., Matsumoto T., Miyake A., Igami Y., Haruta M., Saito H., Hata S., Seto Y., Miyahara M., Tomioka N., Ishii H. A., Bradley J. P., Ohtaki K. K., Dobrică E., Leroux H., Le Guillou C., Jacob D., de la Peña F., Laforet S., Marinova M., Langenhorst F., Harries D., Abreu N. M., Gray J., Zega T., Zanetta P.-M., Thompson M. S., Stroud R., Mathurin J., Dazzi A., Dartois E., Engrand C., Burgess K., Cymes B. A., Bridges J. C., Hicks L., Lee M. R., Daly L., Bland P. A., Zolensky M. E., Frank D. R., Martinez J., Tsuchiyama A., Yasutake M., Matsuno J., Okumura S., Mitsukawa I., Uesugi K., Uesugi M., Takeuchi A., Sun M., Enju S., Takigawa A., Michikami T., Nakamura T., Matsumoto M., Nakauchi Y., Abe M., Nakazawa S., Okada T., Saiki T., Tanaka S., Terui F., Yoshikawa M., Miyazaki A., Nakato A., Nishimura M., Usui T., Yada T., Yurimoto H., Nagashima K., Kawasaki N., Sakamoto N., Hoppe P., Okazaki R., Yabuta H., Naraoka H., Sakamoto K., Tachibana S., Watanabe S. and Tsuda Y. (2024) In situ investigation of an organic micro-globule and its mineralogical context within a Ryugu “sand” grain. *Meteorit. Planet. Sci.* **n/a**.

Phan V. T. H., Rebois R., Beck P., Quirico E., Bonal L. and Noguchi T. (2022) Nanoscale mineralogy and organic structure in Orgueil (CI) and EET 92042 (CR) carbonaceous chondrites studied with AFM-IR spectroscopy. *Meteorit. Planet. Sci.* **57**, 3–21.

Phan V. T. H., Rebois R., Beck P., Quirico E., Noguchi T. and Takase M. (2023) Chemical functional characterization of immature and mature coals at the nanoscale by atomic force microscopy-based infrared spectroscopy (AFM-IR). *Int. J. Coal Geol.* **267**, 104196.

Piani L., Nagashima K., Kawasaki N., Sakamoto N., Bajo K., Abe Y., Aléon J., O'D. Alexander C. M., Amari S., Amelin Y., Bizzarro M., Bouvier A., Carlson R. W., Chaussidon M., Choi B.-G., Dauphas N., Davis A. M., Di Rocco T., Fujiya W., Fukai R., Gautam I., Haba M. K., Hibiya Y., Hidaka H., Homma H., Hoppe P., Huss G. R., Ichida K., Iizuka T., Ireland T. R., Ishikawa A., Itoh S., Kita N. T., Kitajima K., Kleine T., Komatani S., Krot A. N., Liu M.-C., Masuda Y., McKeegan K. D., Morita M., Motomura K., Moynier F., Nakai I., Nguyen A., Nittler L., Onose M., Pack A., Park C., Qin L., Russell S. S., Schönbächler M., Tafla L., Tang H., Terada K., Terada Y., Usui T., Wada S., Wadhwa M., Walker R. J., Yamashita K., Yin Q.-Z., Yokoyama T., Yoneda S., Young

E. D., Yui H., Zhang A.-C., Nakamura T., Naraoka H., Okazaki R., Sakamoto K., Yabuta H., Abe M., Miyazaki A., Nakato A., Nishimura M., Okada T., Yada T., Yogata K., Nakazawa S., Saiki T., Tanaka S., Terui F., Tsuda Y., Watanabe S., Yoshikawa M., Tachibana S. and Yurimoto H. (2023) Hydrogen Isotopic Composition of Hydrous Minerals in Asteroid Ryugu. *Astrophys. J. Lett.* **946**, L43.

Pilorget C., Okada T., Hamm V., Brunetto R., Yada T., Loizeau D., Riu L., Usui T., Moussi-Soffys A., Hatakeyama K., Nakato A., Yogata K., Abe M., Aléon-Toppini A., Carter J., Chaigneau M., Crane B., Gondet B., Kumagai K., Langevin Y., Lantz C., Le Pivert-Jolivet T., Lequerier G., Lourit L., Miyazaki A., Nishimura M., Poulet F., Arakawa M., Hirata N., Kitazato K., Nakazawa S., Namiki N., Saiki T., Sugita S., Tachibana S., Tanaka S., Yoshikawa M., Tsuda Y., Watanabe S. and Bibring J.-P. (2022) First compositional analysis of Ryugu samples by the MicrOmega hyperspectral microscope. *Nat. Astron.*

Pizzarello S. and Holmes W. (2009) Nitrogen-containing compounds in two CR2 meteorites: ^{15}N composition, molecular distribution and precursor molecules. *Geochim. Cosmochim. Acta* **73**, 2150–2162.

Poch O., Istiqomah I., Quirico E., Beck P., Schmitt B., Theulé P., Faure A., Hily-Blant P., Bonal L., Raponi A., Ciarniello M., Rousseau B., Potin S., Brissaud O., Flandinet L., Filacchione G., Pommerol A., Thomas N., Kappel D., Mennella V., Moroz L., Vinogradoff V., Arnold G., Erard S., Bockelée-Morvan D., Leyrat C., Capaccioni F., De Sanctis M. C., Longobardo A., Mancarella F., Palomba E. and Tosi F. (2020) Ammonium salts are a reservoir of nitrogen on a cometary nucleus and possibly on some asteroids. *Science* **367**, eaaw7462.

Potin S., Beck P., Usui F., Bonal L., Vernazza P. and Schmitt B. (2020) Style and intensity of hydration among C-complex asteroids: A comparison to desiccated carbonaceous chondrites. *Icarus* **348**, 113826.

Potin S., Brissaud O., Beck P., Schmitt B., Magnard Y., Correia J.-J., Rabou P. and Jocou L. (2018) SHADOWS: a spectro-gonio radiometer for bidirectional reflectance studies of dark meteorites and terrestrial analogs: design, calibrations, and performances on challenging surfaces. *Appl. Opt.* **57**, 8279–8296.

Potiszil C., Yamanaka M., Sakaguchi C., Ota T., Kitagawa H., Kunihiro T., Tanaka R., Kobayashi K. and Nakamura E. (2023) Organic Matter in the Asteroid Ryugu: What We Know So Far. *Life* **13**.

Quirico E., Bonal L., Kebukawa Y., Amano K., Yabuta H., Phan V. T., Beck P., Rémusat L., Dartois E. and Engrand C. (2023) Compositional heterogeneity of insoluble organic matter extracted from asteroid Ryugu samples. *Meteorit. Planet. Sci.*

Quirico E., Bonal L., Kebukawa Y., Amano K., Yabuta H., Phan V. T. H., Beck P., Rémusat L., Dartois E., Engrand C., Martins Z., Bejach L., Dazzi A., Deniset-Besseau A., Duprat J., Mathurin J., Montagnac G., Barosch J., Cody G. D., De Gregorio B., Enokido Y., Hashiguchi M., Kamide K., Kilcoyne D., Komatsu M., Matsumoto M., Mostefaoui S., Nittler L., Ohigashi T., Okumura T., Sandford S., Shigenaka M., Stroud R., Suga H., Takahashi Y., Takeichi Y., Tamenori Y., Verdier-Paoletti M., Wakabayashi D., Yamashita S., Nakamura T., Naraoka H., Noguchi T., Okazaki R., Yurimoto H., Sakamoto K., Tachibana S., Watanabe S.-I., Tsuda Y., Yada T., Nishimura M., Nakato A., Miyazaki A., Yogata K., Abe M., Okada T., Usui T., Yoshikawa M., Saiki T., Tanaka S., Terui F. and Nakazawa S. (2024) Compositional heterogeneity of insoluble organic matter extracted from asteroid Ryugu samples. *Meteorit. Planet. Sci.* **59**, 1907–1924.

- Rocha W. R. M., Pilling S., Domaracka A., Rothard H. and Boduch P. (2020) Infrared complex refractive index of N-containing astrophysical ices free of water processed by cosmic-ray simulated in laboratory. *Spectrochim. Acta. A. Mol. Biomol. Spectrosc.* **228**, 117826.
- Rojas J., Duprat J., Dartois E., Wu T.-D., Engrand C., Nittler L. R., Bardin N., Delauche L., Mostefaoui S., Remusat L., Stroud R. M. and Guérin B. (2024) Nitrogen-rich organics from comets probed by ultra-carbonaceous Antarctic micrometeorites. *Nat. Astron.*
- Rushdi A. I. and Simoneit B. R. T. (2004) Condensation Reactions and Formation of Amides, Esters, and Nitriles Under Hydrothermal Conditions. *Astrobiology* **4**, 211–224.
- Schmitt-Kopplin P., Hertkorn N., Harir M., Moritz F., Lucio M., Bonal L., Quirico E., Takano Y., Dworkin J. P., Naraoka H., Tachibana S., Nakamura T., Noguchi T., Okazaki R., Yabuta H., Yurimoto H., Sakamoto K., Yada T., Nishimura M., Nakato A., Miyazaki A., Yogata K., Abe M., Usui T., Yoshikawa M., Saiki T., Tanaka S., Terui F., Nakazawa S., Okada T., Watanabe S., Tsuda Y., Hamase K., Furusho A., Hashiguchi M., Fukushima K., Aoki D., Aponte J. C., Parker E. T., Glavin D. P., McLain H. L., Elsila J. E., Graham H. V., Eiler J. M., Ruf A., Orthous-Daunay F.-R., Isa J., Vuitton V., Thissen R., Ogawa N. O., Sakai S., Yoshimura T., Koga T., Sugahara H., Ohkouchi N., Mita H., Furukawa Y., Oba Y., and Hayabusa2-initial-analysis SOM team (2023) Soluble organic matter Molecular atlas of Ryugu reveals cold hydrothermalism on C-type asteroid parent body. *Nat. Commun.* **14**, 6525.
- Sephton M. A. (2002) Organic compounds in carbonaceous meteorites. *Nat. Prod. Rep.* **19**, 292–311.
- Serra C., Vinogradoff V., Danger G., Coulet M.-V. and Duvernay F. (2024) Unexpected mineral impact on organic evolution during simulated aqueous alteration in asteroids. *Icarus* **423**, 116273.
- Shimoyama A. and Ogasawara R. (2002) Dipeptides and Diketopiperazines in the Yamato-791198 and Murchison Carbonaceous Chondrite. *Orig. Life Evol. Biosph.* **32**, 165–179.
- Stroud R. M., Barosch J., Bonal L., Burgess K., Cody G. D., De Gregorio B. T., Daly L., Dartois E., Dobrică E., Duprat J., Engrand C., Harries D., Hashiguchi M., Ishii H., Kebukawa Y., Kilcoyne A. D., Langenhorst F., Lee M. R., Nittler L. R., Quirico E., Okumura T., Remusat L., Sandford S., Yabuta H., Abe M., Abreu N. M., Bagot P. A. J., Beck P., Bejach L., Bland P. A., Bridges J. C., Cymes B. A., Dazzi A., de la Peña F., Deniset-Besseau A., Enju S., Enokido Y., Frank D. R., Gray J., Haruta M., Hata S., Hicks L., Igami Y., Jacob D., Kamide K., Komatsu M., Laforet S., Leroux H., Le Guillou C., Martins Z., Marinova M., Martinez J., Mathurin J., Matsumoto M., Matsumoto T., Matsuno J., McFadzean S., Michikami T., Mitsukawa I., Miyake A., Miyahara M., Miyazaki A., Montagnac G., Mostefaoui S., Nakamura T., Nakato A., Naraoka H., Nakauchi Y., Nakazawa S., Nishimura M., Noguchi T., Ohtaki K., Ohigashi T., Okada T., Okumura S., Okazaki R., Phan T. H. V., Rebois R., Sakamoto K., Saiki T., Saito H., Seto Y., Shigenaka M., Smith W., Suga H., Sun M., Tachibana S., Takahashi Y., Takeichi Y., Takeuchi A., Takigawa A., Tamenori Y., Tanaka S., Terui F., Thompson M. S., Tomioka N., Tsuchiyama A., Tsuda Y., Uesugi K., Uesugi M., Usui T., Verdier-Paoletti M., Wakabayashi D., Watanabe S., Yada T., Yamashita S., Yasutake M., Yogata K., Yoshikawa M., Yurimoto H., Zanetta P.-M., Zega T. and Zolensky M. E. (2024) Electron microscopy observations of the diversity of Ryugu organic matter and its relationship to minerals at the micro- to nano-scale. *Meteorit. Planet. Sci.* **59**, 2023–2043.
- Sugahara H., Takano Y., Tachibana S., Sugawara I., Chikaraishi Y., Ogawa N. O., Ohkouchi N., Kouchi A. and Yurimoto H. (2019) Molecular and isotopic compositions of nitrogen-containing organic molecules formed during UV-irradiation of simulated interstellar ice. *Geochem. J.* **53**, 5–20.

Tachibana S., Sawada H., Okazaki R., Takano Y., Sakamoto K., Miura Y. N., Okamoto C., Yano H., Yamanouchi S., Michel P., Zhang Y., Schwartz S., Thuillet F., Yurimoto H., Nakamura T., Noguchi T., Yabuta H., Naraoka H., Tsuchiyama A., Imae N., Kurosawa K., Nakamura A. M., Ogawa K., Sugita S., Morota T., Honda R., Kameda S., Tatsumi E., Cho Y., Yoshioka K., Yokota Y., Hayakawa M., Matsuoka M., Sakatani N., Yamada M., Kouyama T., Suzuki H., Honda C., Yoshimitsu T., Kubota T., Demura H., Yada T., Nishimura M., Yogata K., Nakato A., Yoshitake M., Suzuki A. I., Furuya S., Hatakeyama K., Miyazaki A., Kumagai K., Okada T., Abe M., Usui T., Ireland T. R., Fujimoto M., Yamada T., Arakawa M., Connolly H. C., Fujii A., Hasegawa S., Hirata N., Hirata N., Hirose C., Hosoda S., Iijima Y., Ikeda H., Ishiguro M., Ishihara Y., Iwata T., Kikuchi S., Kitazato K., Lauretta D. S., Libourel G., Marty B., Matsumoto K., Michikami T., Mimasu Y., Miura A., Mori O., Nakamura-Messenger K., Namiki N., Nguyen A. N., Nittler L. R., Noda H., Noguchi R., Ogawa N., Ono G., Ozaki M., Senshu H., Shimada T., Shimaki Y., Shirai K., Soldini S., Takahashi T., Takei Y., Takeuchi H., Tsukizaki R., Wada K., Yamamoto Y., Yoshikawa K., Yumoto K., Zolensky M. E., Nakazawa S., Terui F., Tanaka S., Saiki T., Yoshikawa M., Watanabe S. and Tsuda Y. (2022) Pebbles and sand on asteroid (162173) Ryugu: In situ observation and particles returned to Earth. *Science* **375**, 1011–1016.

Takano Y., Naraoka H., Dworkin J. P., Koga T., Sasaki K., Sato H., Oba Y., Ogawa N. O., Yoshimura T., Hamase K., Ohkouchi N., Parker E. T., Aponte J. C., Glavin D. P., Furukawa Y., Aoki J., Kano K., Nomura S. M., Orthous-Daunay F.-R., Schmitt-Kopplin P., Furusho A., Hashiguchi M., Fukushima K., Dan Aoki, McLain H. L., Elsila J. E., Graham H. V., Eiler J. M., Hertkorn N., Ruf A., Wolters C., Isa J., Vuitton V., Thissen R., Sakai S., Sugahara H., Mita H., Chikaraishi Y., Yoshikawa T., Tanaka Satoru, Morita M., Onose M., Araoka D., Kabashima F., Fujishima K., Sato H., Yamazaki T., Kimura Y., Yurimoto H., Nakamura T., Noguchi T., Okazaki R., Yabuta H., Sakamoto K., Yada T., Nishimura M., Nakato A., Miyazaki A., Yogata K., Abe M., Okada T., Usui T., Yoshikawa M., Saiki T., Tanaka Satoshi, Terui F., Nakazawa S., Watanabe S., Tsuda Y., Tachibana S., and Hayabusa2-initial-analysis SOM team (2024) Primordial aqueous alteration recorded in water-soluble organic molecules from the carbonaceous asteroid (162173) Ryugu. *Nat. Commun.* **15**, 5708.

Takano Y., Natsushima Y., Yamada K., Okamoto C., Sawada H. and Okazaki R. (2020) Assessment of the explosive chamber in the projector system of Hayabusa2 for asteroid sampling.

Uesugi M., Naraoka H., Ito M., Yabuta H., Kitajima F., Takano Y., Mita H., Ohnishi I., Kebukawa Y., Yada T., Karouji Y., Ishibashi Y., Okada T. and Abe M. (2014) Sequential analysis of carbonaceous materials in Hayabusa-returned samples for the determination of their origin. *Earth Planets Space* **66**, 102.

Vacher L and Phan Thai H.V. (2022): Baseline corrected and normalized mid-IR absorbance spectra of fragments of individual particles C0050 and C0051 (Ryugu samples, Hayabusa2 mission). SSHADE/GhoSST (OSUG Data Center). Dataset/Spectral Data. [doi:10.26302/SSHADE/EXPERIMENT_LB_20241122_002](https://doi.org/10.26302/SSHADE/EXPERIMENT_LB_20241122_002).

Vasylyeva A., Doroshenko I., Vaskivskyi Ye., Chernolevska Ye. and Pogorelov V. (2018) FTIR study of condensed water structure. *J. Mol. Struct.* **1167**, 232–238.

Viennet J., Roskosz M., Nakamura T., Beck P., Baptiste B., Lavina B., Alp E. E., Hu M. Y., Zhao J., Gounelle M., Brunetto R., Yurimoto H., Noguchi T. and Okazaki R. (2023) Interaction between clay minerals and organics in asteroid Ryugu. *Geochem. Perspect. Lett.*, 8–12.

Vollmer C., Leitner J., Kepaptsoglou D., Ramasse Q. M., Busemann H. and Hoppe P. (2020a) Isotopic compositions, nitrogen functional chemistry, and low-loss electron spectroscopy of complex organic aggregates at the nanometer scale in the carbonaceous chondrite Renazzo. *Meteorit. Planet. Sci.* **55**, 1293–1319.

Vollmer C., Leitner J., Kepaptsoglou D., Ramasse Q. M., King A. J., Schofield P. F., Bischoff A., Araki T. and Hoppe P. (2020b) A primordial ^{15}N -depleted organic component detected within the carbonaceous chondrite Maribo. *Sci. Rep.* **10**, 20251.

Wang S., Taraballi F., Tan L. P. and Ng K. W. (2012) Human keratin hydrogels support fibroblast attachment and proliferation in vitro. *Cell Tissue Res.* **347**, 795–802.

Watanabe S., Hirabayashi M., Hirata N., Hirata Na., Noguchi R., Shimaki Y., Ikeda H., Tatsumi E., Yoshikawa M., Kikuchi S., Yabuta H., Nakamura T., Tachibana S., Ishihara Y., Morota T., Kitazato K., Sakatani N., Matsumoto K., Wada K., Senshu H., Honda C., Michikami T., Takeuchi H., Kouyama T., Honda R., Kameda S., Fuse T., Miyamoto H., Komatsu G., Sugita S., Okada T., Namiki N., Arakawa M., Ishiguro M., Abe M., Gaskell R., Palmer E., Barnouin O. S., Michel P., French A. S., McMahon J. W., Scheeres D. J., Abell P. A., Yamamoto Y., Tanaka S., Shirai K., Matsuoka M., Yamada M., Yokota Y., Suzuki H., Yoshioka K., Cho Y., Tanaka S., Nishikawa N., Sugiyama T., Kikuchi H., Hemmi R., Yamaguchi T., Ogawa N., Ono G., Mimasu Y., Yoshikawa K., Takahashi T., Takei Y., Fujii A., Hirose C., Iwata T., Hayakawa M., Hosoda S., Mori O., Sawada H., Shimada T., Soldini S., Yano H., Tsukizaki R., Ozaki M., Iijima Y., Ogawa K., Fujimoto M., Ho T.-M., Moussi A., Jaumann R., Bibring J.-P., Krause C., Terui F., Saiki T., Nakazawa S. and Tsuda Y. (2019) Hayabusa2 arrives at the carbonaceous asteroid 162173 Ryugu—A spinning top-shaped rubble pile. *Science* **364**, 268–272.

Yabuta H., Cody G. D., Engrand C., Kebukawa Y., De Gregorio B., Bonal L., Remusat L., Stroud R., Quirico E., Nittler L., Hashiguchi M., Komatsu M., Okumura T., Mathurin J., Dartois E., Duprat J., Takahashi Y., Takeichi Y., Kilcoyne D., Yamashita S., Dazzi A., Deniset-Besseau A., Sandford S., Martins Z., Tamenori Y., Ohigashi T., Suga H., Wakabayashi D., Verdier-Paoletti M., Mostefaoui S., Montagnac G., Barosch J., Kamide K., Shigenaka M., Bejach L., Matsumoto M., Enokido Y., Noguchi T., Yurimoto H., Nakamura T., Okazaki R., Naraoka H., Sakamoto K., Connolly H. C., Lauretta D. S., Abe M., Okada T., Yada T., Nishimura M., Yogata K., Nakato A., Yoshitake M., Iwamae A., Furuya S., Hatakeyama K., Miyazaki A., Soejima H., Hitomi Y., Kumagai K., Usui T., Hayashi T., Yamamoto D., Fukai R., Sugita S., Kitazato K., Hirata Naru, Honda R., Morota T., Tatsumi E., Sakatani N., Namiki N., Matsumoto K., Noguchi R., Wada K., Senshu H., Ogawa K., Yokota Y., Ishihara Y., Shimaki Y., Yamada M., Honda C., Michikami T., Matsuoka M., Hirata Naoyuki, Arakawa M., Okamoto C., Ishiguro M., Jaumann R., Bibring J.-P., Grott M., Schröder S., Otto K., Pilorget C., Schmitz N., Biele J., Ho T.-M., Moussi-Soffys A., Miura A., Noda H., Yamada T., Yoshihara K., Kawahara K., Ikeda H., Yamamoto Y., Shirai K., Kikuchi S., Ogawa N., Takeuchi H., Ono G., Mimasu Y., Yoshikawa K., Takei Y., Fujii A., Iijima Y., Nakazawa S., Hosoda S., Iwata T., Hayakawa M., Sawada H., Yano H., Tsukizaki R., Ozaki M., Terui F., Tanaka S., Fujimoto M., Yoshikawa M., Saiki T., Tachibana S., Watanabe S. and Tsuda Y. (2023) Macromolecular organic matter in samples of the asteroid (162173) Ryugu. *Science* **379**, eabn9057.

Yada T., Abe M., Okada T., Nakato A., Yogata K., Miyazaki A., Hatakeyama K., Kumagai K., Nishimura M., Hitomi Y., Soejima H., Yoshitake M., Iwamae A., Furuya S., Uesugi M., Karouji Y., Usui T., Hayashi T., Yamamoto D., Fukai R., Sugita S., Cho Y., Yumoto K., Yabe Y., Bibring J.-P., Pilorget C., Hamm V., Brunetto R., Riu L., Lourit L., Loizeau D., Lequertier G., Moussi-Soffys A., Tachibana S., Sawada H., Okazaki R., Takano Y., Sakamoto K., Miura Y. N., Yano H., Ireland T.

R., Yamada T., Fujimoto M., Kitazato K., Namiki N., Arakawa M., Hirata Naru, Yurimoto H., Nakamura T., Noguchi T., Yabuta H., Naraoka H., Ito M., Nakamura E., Uesugi K., Kobayashi K., Michikami T., Kikuchi H., Hirata Naoyuki, Ishihara Y., Matsumoto K., Noda H., Noguchi R., Shimaki Y., Shirai K., Ogawa K., Wada K., Senshu H., Yamamoto Y., Morota T., Honda R., Honda C., Yokota Y., Matsuoka M., Sakatani N., Tatsumi E., Miura A., Yamada M., Fujii A., Hirose C., Hosoda S., Ikeda H., Iwata T., Kikuchi S., Mimasu Y., Mori O., Ogawa N., Ono G., Shimada T., Soldini S., Takahashi T., Takei Y., Takeuchi H., Tsukizaki R., Yoshikawa K., Terui F., Nakazawa S., Tanaka S., Saiki T., Yoshikawa M., Watanabe S. and Tsuda Y. (2022) Preliminary analysis of the Hayabusa2 samples returned from C-type asteroid Ryugu. *Nat. Astron.* **6**, 214–220.

Yada T., Abe M., Okada T., Nakato A., Yogata K., Miyazaki A., Hatakeyama K., Kumagai K., Nishimura M., Hitomi Y., Soejima H., Yoshitake M., Iwamae A., Furuya S., Uesugi M., Karouji Y., Usui T., Hayashi T., Yamamoto D., Fukai R., Sugita S., Cho Y., Yumoto K., Yabe Y., Bibring J.-P., Pilorget C., Hamm V., Brunetto R., Riu L., Lourit L., Loizeau D., Lequertier G., Moussi-Soffys A., Tachibana S., Sawada H., Okazaki R., Takano Y., Sakamoto K., Miura Y. N., Yano H., Ireland T. R., Yamada T., Fujimoto M., Kitazato K., Namiki N., Arakawa M., Hirata Naru, Yurimoto H., Nakamura T., Noguchi T., Yabuta H., Naraoka H., Ito M., Nakamura E., Uesugi K., Kobayashi K., Michikami T., Kikuchi H., Hirata Naoyuki, Ishihara Y., Matsumoto K., Noda H., Noguchi R., Shimaki Y., Shirai K., Ogawa K., Wada K., Senshu H., Yamamoto Y., Morota T., Honda R., Honda C., Yokota Y., Matsuoka M., Sakatani N., Tatsumi E., Miura A., Yamada M., Fujii A., Hirose C., Hosoda S., Ikeda H., Iwata T., Kikuchi S., Mimasu Y., Mori O., Ogawa N., Ono G., Shimada T., Soldini S., Takahashi T., Takei Y., Takeuchi H., Tsukizaki R., Yoshikawa K., Terui F., Nakazawa S., Tanaka S., Saiki T., Yoshikawa M., Watanabe S. and Tsuda Y. (2021) Preliminary analysis of the Hayabusa2 samples returned from C-type asteroid Ryugu. *Nat. Astron.*

Yada T., Fujimura A., Abe M., Nakamura T., Noguchi T., Okazaki R., Nagao K., Ishibashi Y., Shira K., Zolensky M. E., Sandford S., Okada T., Uesugi M., Karouji Y., Ogawa M., Yakame S., Ueno M., Mukai T., Yoshikawa M. and Kawaguchi J. (2014) Hayabusa-returned sample curation in the Planetary Material Sample Curation Facility of JAXA. *Meteorit. Planet. Sci.* **49**, 135–153.

Yesiltas M., Glotch T. D., Kebukawa Y., Sava B., Durmaz Y. C. and Northrup P. (2024) Nanoscale Spectroscopic Identification and Characterization of Minerals and Organic Matter in Ryugu Particles. *J. Geophys. Res. Planets* **129**, e2023JE008090.

Yoshimura T., Takano Y., Naraoka H., Koga T., Araoka D., Ogawa N. O., Schmitt-Kopplin P., Hertkorn N., Oba Y., Dworkin J. P., Aponte J. C., Yoshikawa T., Tanaka Satoru, Ohkouchi N., Hashiguchi M., McLain H., Parker E. T., Sakai S., Yamaguchi M., Suzuki T., Yokoyama T., Yurimoto H., Nakamura T., Noguchi T., Okazaki R., Yabuta H., Sakamoto K., Yada T., Nishimura M., Nakato A., Miyazaki A., Yogata K., Abe M., Okada T., Usui T., Yoshikawa M., Saiki T., Tanaka Satoshi, Terui F., Nakazawa S., Watanabe S., Tsuda Y., Tachibana S., Hamase K., Furusho A., Fukushima K., Aoki D., Glavin D. P., McLain H. L., Elsila J. E., Graham H. V., Eiler J. M., Ruf A., Orthous-Daunay F.-R., Wolters C., Isa J., Vuitton V., Thissen R., Sugahara H., Mita H., Furukawa Y., Chikaraishi Y., Morita M., Onose M., Kabashima F., Fujishima K., Sato H., Sasaki K., Kano K., Nomura S. M., Aoki J., Yamazaki T., Kimura Y., and Hayabusa2-initial-analysis SOM team (2023) Chemical evolution of primordial salts and organic sulfur molecules in the asteroid 162173 Ryugu. *Nat. Commun.* **14**, 5284.

Supplementary Information for

**NH-rich organic compounds from the carbonaceous asteroid (162173)
Ryugu: nanoscale spectral and isotopic characterizations**

*L. G. Vacher¹, V. T. H. Phan¹, L. Bonal¹, M. Iskakova², O. Poch¹, P. Beck¹, E. Quirico¹, & R. C. Ogliore²

*Corresponding author: lionel.vacher@univ-grenoble-alpes.fr

¹Univ. Grenoble Alpes, CNRS, IPAG, 38000 Grenoble, France

²Department of Physics, Washington University in St. Louis, St. Louis, MO, USA.

Submitted to *Meteoritics and Planetary Science* – December 26, 2024

S1. Selection of Ryugu's particles based on FTIR spectra from Ryugu Sample Database System

First, we collected all the FTIR spectra of Ryugu particles available for AO allocation from the Ryugu Sample Database, as of January 2022 (<https://darts.isas.jaxa.jp/app/curation/ryugu/>). Next, we identified particles lacking strong carbonate absorption bands at $\sim 3.8\text{--}4.0 \mu\text{m}$ to mitigate spectral ambiguities, as carbonate and NH_4^+ salts can exhibit similar absorption patterns at $\sim 3.4 \mu\text{m}$ (Lin-Vien et al., 1991; Petit et al., 2006). Based on this criterium, we identified two particles from Chamber A and three from Chamber C that had weak or absent carbonate absorption bands: A0093, A0099, C0050, C0052, and C0083 (Figure S1). We baseline-corrected all the spectra using two approaches: baseline correction n°1 used four correction points at $2.64 \mu\text{m}$, $2.88 \mu\text{m}$, $3.62 \mu\text{m}$, and $3.88 \mu\text{m}$, while baseline correction n°2 used six correction points at $2.64 \mu\text{m}$, $2.88 \mu\text{m}$, $3.16\text{--}3.25 \mu\text{m}$, $3.62 \mu\text{m}$, and $3.88 \mu\text{m}$, similar to Yada et al. (2021) (Figure S1). Among these selected spectra, particles A0099 and C0083 showed absorption bands possibly attributed to $\text{N-H}/\text{NH}_4^+$ in phyllosilicates ($3.03\text{--}3.05 \mu\text{m}$) and aliphatic/aromatic organic compounds ($3.38\text{--}3.5 \mu\text{m}$). In contrast, particles C0050, C0052, and A0093 displayed broader and deeper absorption features from $3.03 \mu\text{m}$ to $3.3 \mu\text{m}$, suggesting the presence of $\text{N-H}/\text{NH}_4^+$ in a more diverse range of compounds or environments, including phyllosilicates, salts, and aliphatic/aromatic organic compounds ($3.38\text{--}3.5 \mu\text{m}$). Following our proposal, the JAXA curation team allocated particles C0050 and C0052.

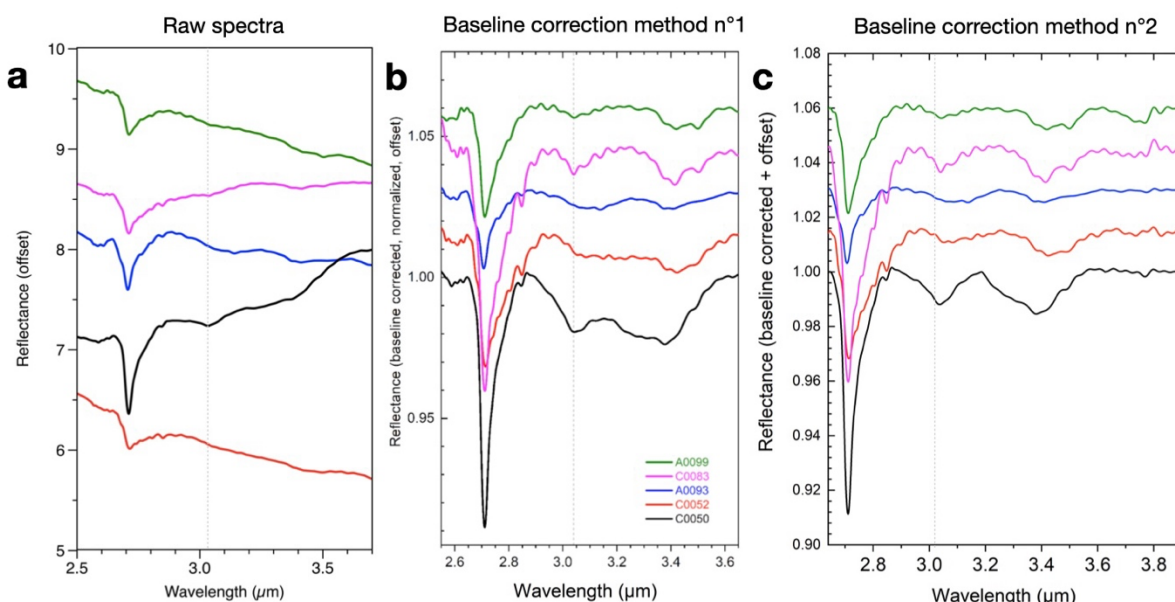


Figure S1. FTIR reflectance spectra (raw and baseline-corrected) between $2.6 \mu\text{m}$ to $3.6 \mu\text{m}$ of Ryugu particles A0093 (blue), A0099 (green), C0050 (black), C0052 (red), and C0083 (pink) from the Ryugu Sample Database System showing absorption bands at $\sim 3.05 \mu\text{m}$ and $\sim 3.4 \mu\text{m}$ attributed to NH/NH_4^+ -bearing compounds and organic molecules/carbonate, respectively. (a) The raw FTIR spectra from the Ryugu Sample Database. (b) The FTIR spectra were baseline-corrected at $2.64 \mu\text{m}$, $2.88 \mu\text{m}$, $3.62 \mu\text{m}$ and $3.88 \mu\text{m}$ (baseline correction n°1), resulting in a broad absorption feature between $\sim 2.9 \mu\text{m}$ to $\sim 3.6 \mu\text{m}$. (c) The FTIR spectra were baseline-corrected at $2.64 \mu\text{m}$, $2.88 \mu\text{m}$, $3.16 \mu\text{m}$ to $3.25 \mu\text{m}$, $3.62 \mu\text{m}$,

and $3.88\text{ }\mu\text{m}$ (baseline correction n°2) similar to Yada et al. (2021). The vertical grey dotted line corresponds to the absorption band at $\sim 3.05\text{ }\mu\text{m}$.

S2. SEM-EDS measurements

Following AFM-IR analysis, the samples were coated with a thin gold film for observation using a scanning electron microscope (SEM) in secondary and backscattered electron (BSE) modes. The SEM analysis were conducted with a JEOL JSM-7000F, equipped with energy-dispersive spectroscopy (EDS), at the Consortium des Moyens Technologiques Communs (CMTC) at University Grenoble Alpes, France. EDS mapping of C, O, Si, Mg, Fe, N and Al was performed using an acceleration voltage of 10 kV and a beam current of 30 nA. EDS spectra were also collected to further analyse the elemental composition of NH-bearing compounds.

BSE image and EDS composite maps of C, Si, and Fe (Figure S2) revealed N-rich regions, corresponding to areas of strong absorption at 1660 cm^{-1} and 1550 cm^{-1} , as identified by AFM-IR (Figure 2). The EDS spectra showed higher concentrations of C, O, Mg, Fe, and Si in spots S1 and S3 compared to S2 and S4 (Figures S2-E and S2-F). In contrast, small N peaks were detected in spots S2 and S4, consistent with the presence of amides identified through AFM-IR analysis.

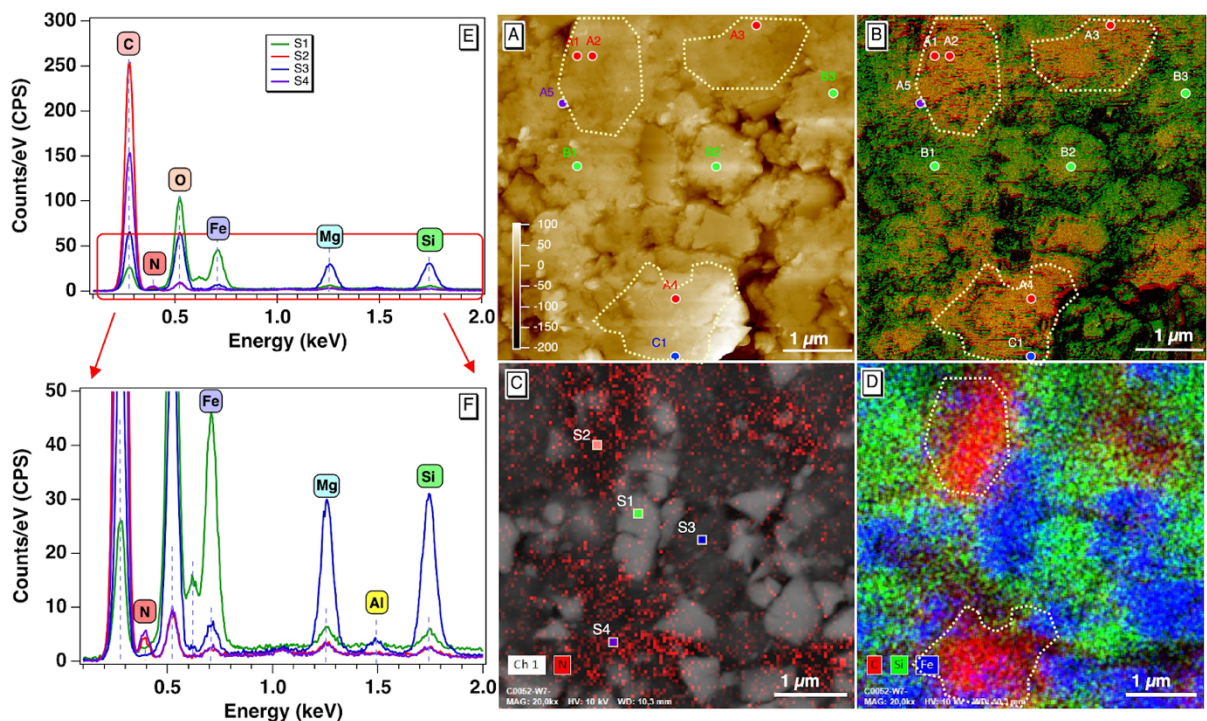


Figure S2. (A-B) AFM and RGY composite images using the APE laser in the area showing the combined absorption bands at R = 1660 cm^{-1} ; G = 1000 cm^{-1} , Y = 1550 cm^{-1} . (C) The SEM map mixed with the nitrogen (N) signature in the same area as AFM-IR shown in (A)-(B), and (D) the EDX analysis showing the composition map of C (red), Fe (blue) and Si (green) in the SEM image of C0052 grain. (E-F) EDS spectra and zoom of EDS spectra of the locations shown in the SEM map (C) labelled S1-S4.

S4 showing the presence of N in S2 and S4 where N-H organic compounds are found via AFM-IR analysis.

S3. Location of NH-rich regions in particle C0052 analyzed by μ -FTIR

We prepared and analyzed multiple $100 \times 100 \mu\text{m}^2$ areas of crushed fragments from particles C0050 and C0052 using μ -FTIR, both under N_2 and atmospheric conditions. Among these analyses, only a few areas from particle C0052 exhibited a broad band at $\sim 3250 \text{ cm}^{-1}$, which overlaps with the main asymmetric stretch vibration mode of NH_4^+ ($\sim 3250 \text{ cm}^{-1}$). In Figure S3, we present the optical image of window #7 analyzed under atmospheric conditions, highlighting the locations of our μ -FTIR analyses and, for some of them, their associated spectra. The areas investigated by AFM-IR, where the amides were detected at the micrometer-scale (7-G1-3 and 7-G2-1), are marked by colored arrows. It is important to note that the broad band at $\sim 3250 \text{ cm}^{-1}$ may also result from contribution of water ice deposited on the infrared detector, so we systematically performed a background measurement before each analysis to minimize this potential instrumental artifact.

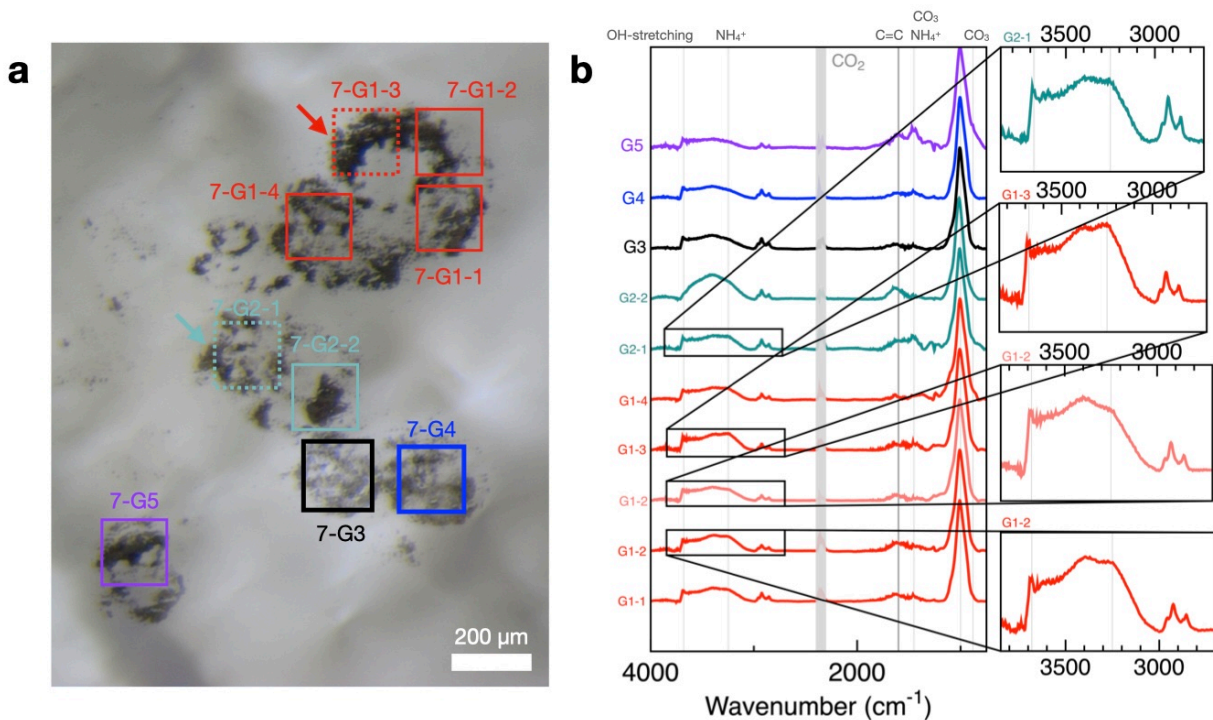


Figure S3. (a) Optical image of the surface of diamond window #7, where fragments of Ryugu's particle C0052 were crushed for μ -FTIR analyses under atmospheric conditions. The colored squares represent the $100 \times 100 \mu\text{m}^2$ areas analyzed by μ -FTIR. The colored arrows indicate the areas (7-G1-3 and 7-G2-1) where samples exhibit a broad band at $\sim 3250 \text{ cm}^{-1}$, possibly corresponding to the asymmetric stretch vibration mode of NH_4^+ , and where NH-rich compounds were detected by AFM-IR. (b) μ -FTIR spectra (normalized to 1000 cm^{-1}) corresponding to some of the areas shown in panel (a).

S4. AFM-IR measurements of the NH-rich compounds

In addition to the 7-G2-1 region, another area in the 7-G1-3 grain (Figure S3) shows characteristic double peaks at 1660 cm^{-1} and 1550 cm^{-1} (Figure S4). AFM-IR images were captured at different wavenumbers: 1720 cm^{-1} (C=O stretching), 1450 cm^{-1} (CH_2 bending or carbonate) and 1000 cm^{-1} (Si-O stretching). Although IR absorption images were not obtained at 1660 and 1550 cm^{-1} , three maps at these three wavenumbers, combined into composite RGB images, helped identify two distinct domains (Figure S4). The first domain shows strong absorption at 1000 cm^{-1} , typical of phyllosilicates found in Ryugu or CI chondrites. The second domain, covering most of the image, has a dominant absorption at 1720 cm^{-1} , attributed to carbonyl (C=O) and associated with OM. Approximately 50 AFM-IR spectra collected across the second region revealed two distinct zones: the first zone, exhibits a narrow, and variable feature near 1000 cm^{-1} , indicative of phyllosilicates; while the second zone displays N-related organic signatures at 1720 cm^{-1} , 1660 cm^{-1} , and 1550 cm^{-1} .

In contrast to 7-G2-1, the 1720 cm^{-1} peak is more prominent in 7-G1-3, reflecting a stronger carbonyl (C=O) stretching band. Some spectra display the double peaks at 1660 cm^{-1} and 1550 cm^{-1} (similar to 7-G2-1), while others only show peaks in 1720 cm^{-1} and 1660 cm^{-1} . All organic matter-related spectra exhibit a peak at 1450 cm^{-1} , attributed to CH_2 bending rather than carbonate. This conclusion is supported by the absence of the 880 cm^{-1} peak, which corresponds to the in-plane mode of carbonate mode. Furthermore, the polycyclic (C=C) feature, typically observed near 1600 cm^{-1} , is weak or absent, likely masked by the dominant 1660 cm^{-1} feature.

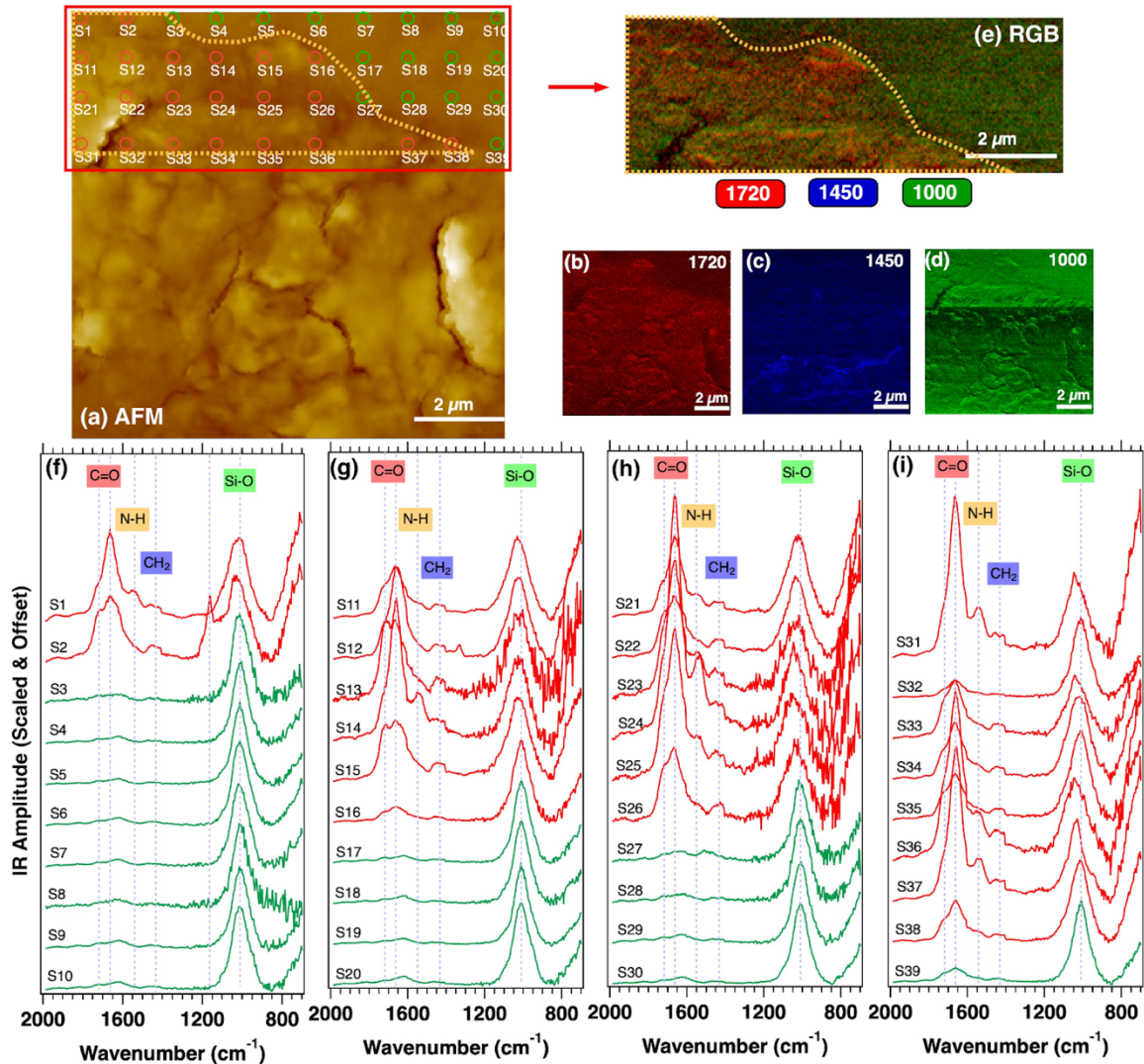


Figure S4. AFM-IR tapping mode maps using the APE laser ($2000\text{--}700\text{ cm}^{-1}$) of the 7-G1-3 region with (a) AFM image from particle C0052 with the location of single-point AFM-IR spectra at absorption bands of (b) 1720 cm^{-1} (C=O from organic matter) and (c) 1450 cm^{-1} (CH_2 bending mode); and (d) 1000 cm^{-1} (phyllosilicates); and (e) combined RGB map ($R = 1720\text{ cm}^{-1}$; $G = 1000\text{ cm}^{-1}$, $B = 1450\text{ cm}^{-1}$). The organic-rich region is highlighted by orange dashed lines. AFM-IR contact spectra associated with different positions located in the AFM topographic map, (f) AFM-IR spectra of S1–S10, (g) AFM-IR spectra of S11–S20, (h) AFM-IR spectra of S21–S30, (i) AFM-IR spectra of S31–S39.

The 7-G2-1 region in C0052 ($5 \times 5\text{ }\mu\text{m}^2$) containing the amides was also analyzed in contact mode (CM) using the FF laser across the $3800\text{--}2700\text{ cm}^{-1}$ range (Figure S5). AFM-IR images were obtained at 2930 cm^{-1} (red), 2960 cm^{-1} (pink), 3240 cm^{-1} (blue) and 3680 cm^{-1} (green) corresponding respectively to 2930 cm^{-1} and 2960 cm^{-1} , the asymmetric stretching modes of $-\text{CH}_2$ and $-\text{CH}_3$ groups in organic matter (OM), 3240 cm^{-1} , possible $-\text{N-H}$ stretching mode and 3680 cm^{-1} , $-\text{OH}$ stretching mode from phyllosilicate. The compositional map was generated by combining images at 2930 cm^{-1} , 3680 cm^{-1} and 3240 cm^{-1} . This region showed a significant contribution of $-\text{OH}$ stretching at 3680 cm^{-1} .

¹ and strong absorption at 2930 cm⁻¹ and 2960 cm⁻¹, highlighting aliphatic asymmetric stretching modes in organic matter (OM). Additionally, absorption at 1000 cm⁻¹, observed using the APE laser in the 2000–700 cm⁻¹ range within the same region of interest (ROI), confirmed the presence of phyllosilicates.

When comparing the CH₂/CH₃ ratios from regions A and B with the μ -FTIR spectra of C0052 grain and the spectrum of the insoluble organic matter (IOM) extracted from C0057 grain (Quirico et al., 2023), the observed CH₂/CH₃ ratios were 0.77, 0.85, and 0.72, respectively. This comparison highlights the notable consistency in the chain lengths of the CH₂/CH₃ groups.

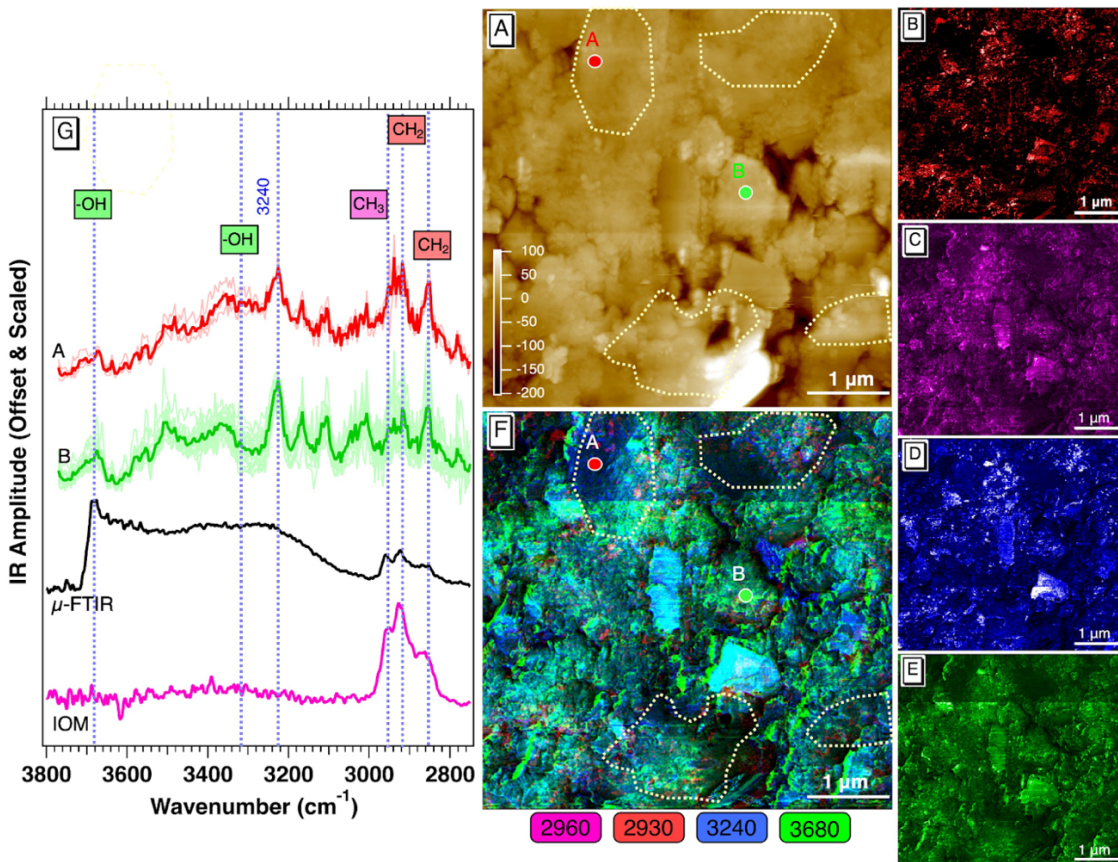


Figure S5. AFM-IR tapping mode maps using the FF laser ($4000\text{--}2700\text{ cm}^{-1}$) of the region 7-G2-1 analyzed using the APE laser (Figure 3). (A) Topographical image. (B) Aliphatic CH_2 asymmetric stretching at 2930 cm^{-1} (red). (C) Aliphatic CH_3 asymmetric stretching at 2960 cm^{-1} (pink). (D) Possible N-H stretching at 3240 cm^{-1} . (E) -OH stretching at 3680 cm^{-1} . (F) RGB (Red, Green, Blue) composite image of the three maps: 2930 cm^{-1} , 3680 cm^{-1} and 3240 cm^{-1} , respectively. (G) AFM-IR contact spectra associated with regions A (red) and B (green) located in the AFM topographic map, compared to the μ -FTIR spectra of C0052 grain (black) and the insoluble organic matter (IOM) extracted from the C0057 grain (pink, Quirico et al. 2023). The vertical blue dashed lines highlight the characteristic band positions of -OH from phyllosilicates, aliphatic signatures ($\text{CH}_2\text{-CH}_3$) from organic matter, and N-H stretching mode at 3240 cm^{-1} from amide compounds.

Table S1. List of all AFM-IR and NanoSIMS analyzed areas for Ryugu sample C0052, along with the detected compounds (e.g., Si-O for phyllosilicates, N-H, organic materials, and CO₃²⁻ for carbonates). Highlighted results indicate the total area corresponding to the amides analyzed by NanoSIMS, and their resulting calculated proportion in the Ryugu grain C0052.

Samples	Vibration mode identified	Area analyzed (μm ²)
AFM-IR		
7-G1-3_1	Only Si-O	400
7-G1-3_2	Only Si-O	400
7-G1-3_3	Si-O, N-H	400
7-G1-3_4	Si-O, N-H	100
7-G1_3*	N-H	30
7-G1-3_1	CO ₃ , Si-O	400
7-G1-3_2	organics, CO ₃ , Si-O	400
7-G2-1	Si-O, N-H	100
10-G1	CO ₃ , Si-O	400
10-G3	organics, Si-O	400
10-G6	CO ₃ , Si-O	400
10-G6	CO ₃ , Si-O, olivine	100
Total AFM-IR areas C0052		3530
Total amide areas detected in C0052 (AFM-IR)		30
Total NanoSIMS areas C0052 (5 x 5 μm ²)		200
Total amide areas in C0052 (C and N by NanoSIMS)[§]		5.6
vol.% NH-organic compound in C0052		0.96

*Area of the 1720 cm⁻¹ region in Figure S4.

[§]Sum of all ROIs analyzed by NanoSIMS. This estimated also included the 7-G2-1 AFM-IR area (equivalent to ROIs 1 to 4 in NanoSIMS) where the amides have been detected (Figure 3).

Table A2. List of all AFM-IR analysed areas for Ryugu sample C0050.

Samples	Vibration mode identified	Area analyzed (μm^2)
3-G1-1	organics, CO_3 , Si-O	400
3-G1-2	Only Si-O	100
3-G2	Si-O, olivine	400
3-G3-1	organics, Si-O	100
3-G3-2	organics, CO_3 , Si-O	500
4-G1-1	Only Si-O	125
4-G1-3	organics, Si-O	464
4-G1-4	Only Si-O	25
6-G1-1	CO_3 , Si-O	900
6-G1-4	organics, Si-O	416
6-G2-1	organics, Si-O	416
Total AFM-IR areas C0050		3846

S5. NanoSIMS measurements and standard corrections

The instrumental mass fractionation (IMF) for C, N, and H isotopes was calculated using the weighted mean of all measurements of the reference material throughout the analytical session (Figure S6). The IMF correction was then applied to the unknown sample following a standards-based correction that minimize the quasi-simultaneous arrival (QSA) effects when using electron multiplier detectors (see equation 23 in Ogliore et al. 2021). The total uncertainties for each ROI on the unknown sample were estimated as the square sum of the reference material reproducibility and the internal precision of each ROI on the sample (given by the Poisson error).

Given the depletion in ^{15}N of the amides, we systematically checked the applied central line (CL) values (determined by high mass resolution (HMR) scans before each analysis) for the deflection plates of the ^{13}C and $^{12}\text{C}^{15}\text{N}$ detectors between the reference material and the unknown samples (gray areas, Figure S6a–e). A shift in CL value between the kerogen and the unknown sample could cause a systematic depletion (or enrichment) in ^{15}N in the unknown sample. However, the CL values obtained for the unknown sample differ from the kerogen standard by less than one volt. Therefore, we believe the ^{15}N depletion measured in the amides in Ryugu does not result from instrumental artifacts.

The NanoSIMS search was conducted on multiple $5 \times 5 \mu\text{m}^2$ areas surrounding region 7-G2-1, where N-H organic compounds were detected by AFM-IR (Figure 3). Although we only identified the amides by AFM-IR in the corresponding NanoSIMS areas 1 and 2, we assumed that the surrounding areas (3 and 4), which also show $^{12}\text{C}^{14}\text{N}^-$ -rich regions of similar size and $^{12}\text{C}^{14}\text{N}^-$ count rates, consist of the same phase (Figure S7). Because C-N and H isotopes were acquired during two separate sessions, we systematically checked the last cycle of $^{12}\text{C}^{14}\text{N}^-$ from the first session ($^{12}\text{C}^-$, $^{13}\text{C}^-$, $^{12}\text{C}^{14}\text{N}^-$, $^{12}\text{C}^{15}\text{N}^-$ and $^{28}\text{Si}^-$) and the first cycle of $^1\text{H}^-$ images from the second session (H^- and D^-) to locate the N-H organic compounds due to sample consumption and define ROIs for H isotope analysis (when applicable). The NanoSIMS areas 5 to 8 do not contain sufficient $^{12}\text{C}^{14}\text{N}^-$ -rich regions for precise isotopic characterization, so they are not reported in Table 1.

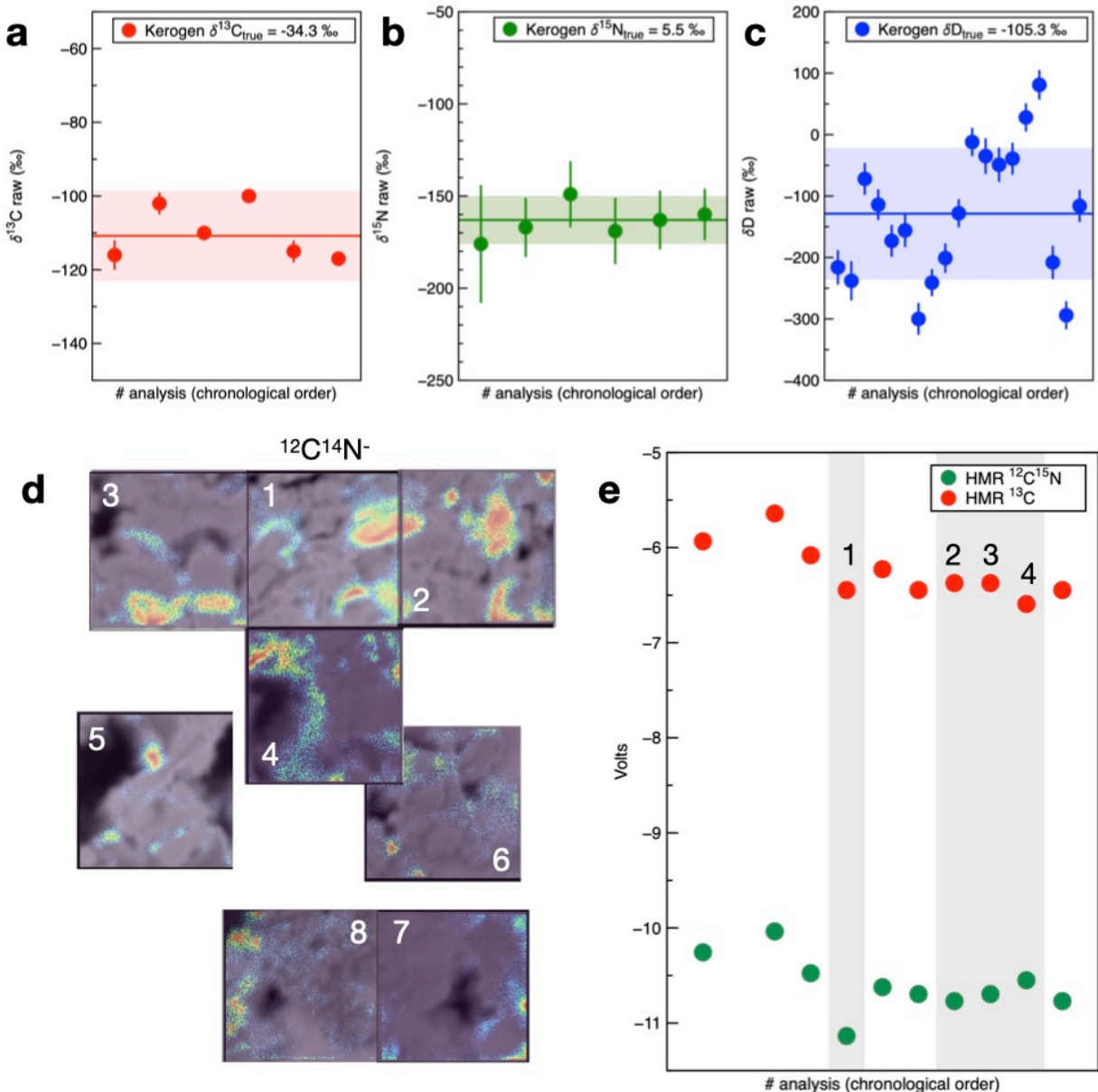


Figure S6. (a-c) C, N, and H isotopic reproducibility of the kerogen standards across the analytical session. The colored solid lines indicate the calculated weighted mean, and the associated shaded areas represent the 1σ uncertainty. (d) NanoSIMS accumulated images ($5 \times 5 \mu\text{m}^2$) of $^{12}\text{C}^{14}\text{N}^-$ ions from area 7-G2-1 of particle C0052, showing the spatial distribution of NH-rich compounds detected by AFM-IR in images 1 and 2. The $^{12}\text{C}^{14}\text{N}^-$ -rich regions in analyzed areas (3 and 4) are assumed to correspond to the NH-rich phase. The numbers indicate the chronological order of the analyses. (e) Central line (CL) values determined during high mass resolution (HMR) scans applied to the deflection plates of detectors for ^{13}C and $^{12}\text{C}^{15}\text{N}$ for the kerogen standard (white areas) and samples (gray areas). The corresponding numbers refer to the analyzed areas shown in panel (d).

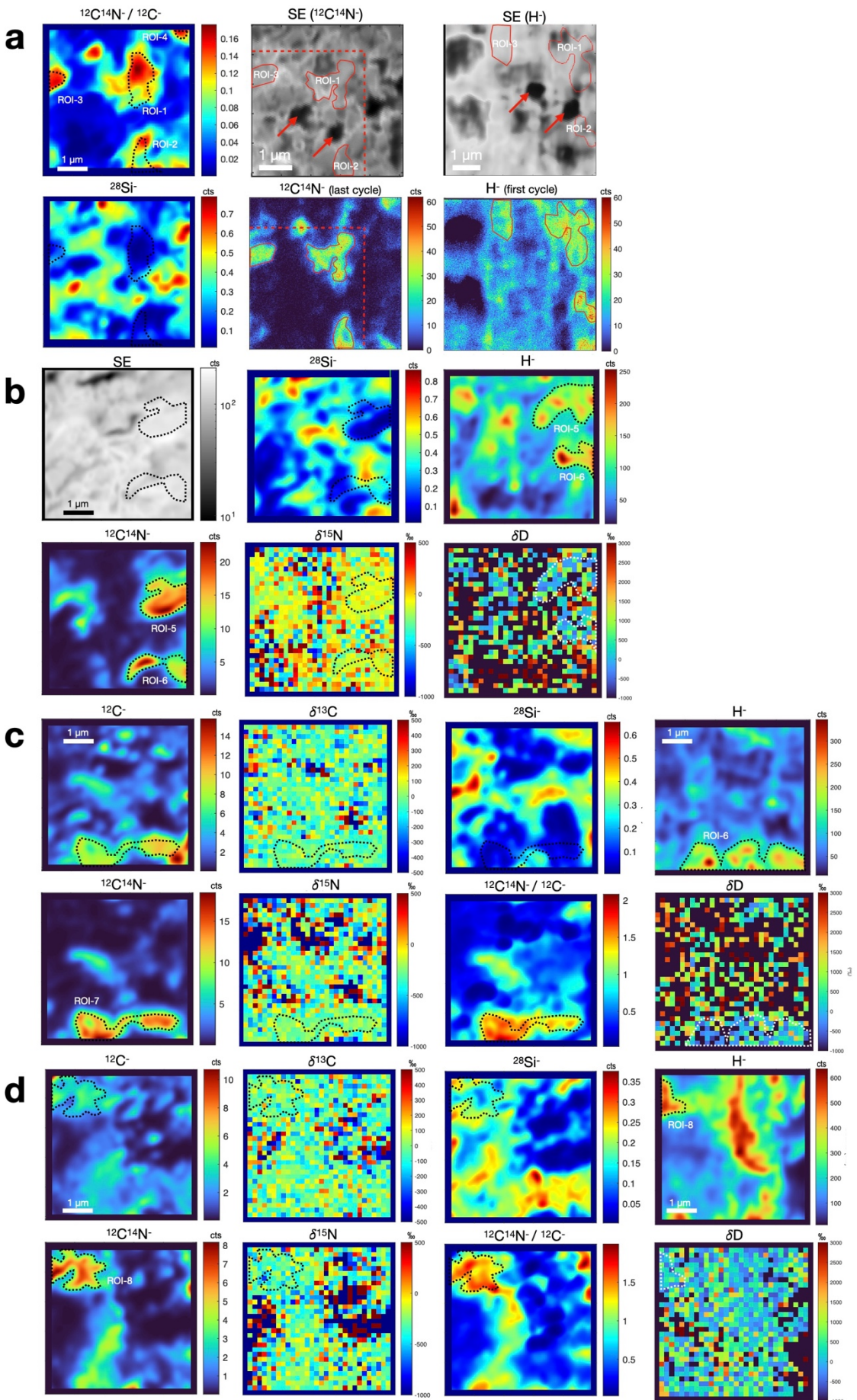


Figure S7. NanoSIMS accumulated images ($5 \times 5 \mu\text{m}^2$) of secondary electron (SE), $^{12}\text{C}^-$, $^{12}\text{C}^{14}\text{N}^-$, $^{12}\text{C}^{14}\text{N}^-/^{12}\text{C}$, $^{28}\text{Si}^-$ and $^1\text{H}^-$ ions, $\delta^{13}\text{C}$, as well as $\delta^{15}\text{N}$ and δD in different $5 \times 5 \mu\text{m}^2$ areas of the 7-G2-1 region from particle C0052 (Figure 3). ROIs corresponding to amides detected by AFM-IR are outlined by black or white dashed lines. (a) NanoSIMS accumulated and single cycle images of SE, $^{12}\text{C}^{14}\text{N}^-/^{12}\text{C}$ and $^{28}\text{Si}^-$, $^{12}\text{C}^{14}\text{N}^-$ and $^1\text{H}^-$ ions for ROIs 1 to 4 (Figure 4). Due to sample consumption after the first session, accumulated SE, the last cycle of $^{12}\text{C}^{14}\text{N}^-$, and the first cycle of $^1\text{H}^-$ images were used to locate the remaining NH-rich organic compounds and select them as the ROI for H isotope analysis. Red arrows indicate similar characteristics between the two SE images from both sessions, highlighting the remaining N-H organic compounds (marked by red ROIs). Red dashed lines indicate the location of the H area analysis. (b) NanoSIMS accumulated images of SE, $^{12}\text{C}^{14}\text{N}^-$, $^{28}\text{Si}^-$ and $^1\text{H}^-$, $\delta^{15}\text{N}$ and δD for ROIs 5 and 6. The C isotopic analysis is not shown due to analytical issues. However, ROI-5 corresponds to the continuation of ROI-3 in (a) and should therefore be similar. (c-d) NanoSIMS accumulated $^{12}\text{C}^-$, $^{12}\text{C}^{14}\text{N}^-$, $^{28}\text{Si}^-$, $^{12}\text{C}^{14}\text{N}^-/^{12}\text{C}$, $^1\text{H}^-$ ions, as well as $\delta^{13}\text{C}$, $\delta^{15}\text{N}$ and δD for ROIs 7 to 8.

References

- Lin-Vien D., Colthup N. B., Fateley W. G. and Grasselli J. G. (1991) *The handbook of infrared and Raman characteristic frequencies of organic molecules.*, Elsevier.
- Ogliore R., Nagashima K., Huss G. and Haenecour P. (2021) A reassessment of the quasi-simultaneous arrival effect in secondary ion mass spectrometry. *Nucl. Instrum. Methods Phys. Res. Sect. B Beam Interact. Mater. At.* **491**, 17–28.
- Petit S., Righi D. and Madejová J. (2006) Infrared spectroscopy of NH_4^+ -bearing and saturated clay minerals: A review of the study of layer charge. *Layer Charge Clay Miner.* **34**, 22–30.
- Quirico E., Bonal L., Kebukawa Y., Amano K., Yabuta H., Phan V. T., Beck P., Rémusat L., Dartois E. and Engrand C. (2023) Compositional heterogeneity of insoluble organic matter extracted from asteroid Ryugu samples. *Meteorit. Planet. Sci.*
- Yada T., Abe M., Okada T., Nakato A., Yogata K., Miyazaki A., Hatakeyama K., Kumagai K., Nishimura M., Hitomi Y., Soejima H., Yoshitake M., Iwamae A., Furuya S., Uesugi M., Karouji Y., Usui T., Hayashi T., Yamamoto D., Fukai R., Sugita S., Cho Y., Yumoto K., Yabe Y., Bibring J.-P., Pilorget C., Hamm V., Brunetto R., Riu L., Lourit L., Loizeau D., Lequertier G., Moussi-Soffys A., Tachibana S., Sawada H., Okazaki R., Takano Y., Sakamoto K., Miura Y. N., Yano H., Ireland T. R., Yamada T., Fujimoto M., Kitazato K., Namiki N., Arakawa M., Hirata Naru, Yurimoto H., Nakamura T., Noguchi T., Yabuta H., Naraoka H., Ito M., Nakamura E., Uesugi K., Kobayashi K., Michikami T., Kikuchi H., Hirata Naoyuki, Ishihara Y., Matsumoto K., Noda H., Noguchi R., Shimaki Y., Shirai K., Ogawa K., Wada K., Senshu H., Yamamoto Y., Morota T., Honda R., Honda C., Yokota Y., Matsuoka M., Sakatani N., Tatsumi E., Miura A., Yamada M., Fujii A., Hirose C., Hosoda S., Ikeda H., Iwata T., Kikuchi S., Mimasu Y., Mori O., Ogawa N., Ono G., Shimada T., Soldini S., Takahashi T., Takei Y., Takeuchi H., Tsukizaki R., Yoshikawa K., Terui F., Nakazawa S., Tanaka S., Saiki T., Yoshikawa M., Watanabe S. and Tsuda Y. (2021) Preliminary analysis of the Hayabusa2 samples returned from C-type asteroid Ryugu. *Nat. Astron.*